Pergamon

Geochimica et Cosmochimica Acta, Vol. 68, No. 5, pp. 1115–1133, 2004

0016-7037/04 $30.00 + .00

doi:10.1016/j.gca.2003.08.006

Geochemical models of metasomatism in ultramafic systems: Serpentinization, rodingitization, and sea floor carbonate chimney precipitation

JAMES L. PALANDRI* and MARK H. REED
U.S. Geological Survey, 345 Middlefield Rd., MS 427, Menlo Park, CA 94025, USA

(*Received April* 9, 2003; *accepted in revised form August* 15, 2003)

Abstract—In a series of water-rock reaction simulations, we assess the processes of serpentinization of harzburgite and related calcium metasomatism resulting in rodingite-type alteration, and seafloor carbonate chimney precipitation. At temperatures from 25 to 300°C (P = 10 to 100 bar), using either fresh water or seawater, serpentinization simulations produce an assemblage commonly observed in natural systems, dominated by serpentine, magnetite, and brucite. The reacted waters in the simulations show similar trends in composition with decreasing water-rock ratios, becoming hyper-alkaline and strongly reducing, with increased dissolved calcium. At 25°C and w/r less than ~32, conditions are sufficiently reducing to yield H_2 gas, nickel-iron alloy and native copper. Hyperalkalinity results from OH^- production by olivine and pyroxene dissolution in the absence of counterbalancing OH^- consumption by alteration mineral precipitation except at very high pH; at moderate pH there are no stable calcium minerals and only a small amount of chlorite forms, limited by aluminum, thus allowing Mg^{2+} and Ca^{2+} to accumulate in the aqueous phase in exchange for H^+. The reducing conditions result from oxidation of ferrous iron in olivine and pyroxene to ferric iron in magnetite. Trace metals are computed to be nearly insoluble below 300°C, except for mercury, for which high pH stabilizes aqueous and gaseous Hg°. In serpentinization by seawater at 300°C, Ag, Au, Pd, and Pt may approach ore-forming concentrations in sulfide complexes. Simulated mixing of the fluid derived from serpentinization with cold seawater produces a mineral assemblage dominated by calcite, similar to recently discovered submarine, ultramafic rock-hosted, carbonate mineral deposits precipitating at hydrothermal vents. Simulated reaction of gabbroic or basaltic rocks with the hyperalkaline calcium- and aluminum-rich fluid produced during serpentinization at 300°C yields rodingite-type mineral assemblages, including grossular, clinozoisite, vesuvianite, prehnite, chlorite, and diopside.

1. INTRODUCTION

Hydrothermal alteration of peridotite produces serpentinites in both submarine and terrestrial environments, and is a step in the formation of rodingites. Serpentinization is an exothermic, hydration reaction whereby water reacts with mafic minerals such as olivine and pyroxene, to produce lizardite, antigorite, and/or chrysotile. Rodingites are altered, calcium-enriched, country rocks that are in contact with altered peridotites; protoliths include basalt, gabbro, mafic cumulates, volcanic rocks, granitic rocks, serpentinites, or sediments. Rodingites are formed by the migration of calcium carried in serpentinizing fluids from peridotite into country rock.

In this study we compute multicomponent equilibria to assess some of the chemical effects of reacting peridotite with meteoric water and seawater at 25 to 300°C (P = 10 to 100 bar). We identify the chemical reactions that lead to high fluid pH and highly reducing conditions. Once these processes are well defined, we address the response of minor and trace elements, and the constraints upon their leaching from ultramafic rock. Previous theoretical investigations of submarine hydrothermal systems by Wetzel and Shock (2000) use various rock compositions containing 12 major and minor elements, for modeling separately serpentinization and basalt alteration by seawater. Our investigation addresses 25 elements including several trace metals of economic interest, including Ni, Cu, Ag, Au, Hg, Co, Pd, and Pt. Additional simulations address mixing of the fluid product of serpentinization with cold seawater, and rodingite alteration, both of which are related to serpentinization.

* Author to whom correspondence should be addressed (jlpaland@usgs.gov).

2. MATERIAL AND METHODS

2.1. Overview of the Technique

Calculations are performed with the FORTRAN computer programs SOLVEQ and CHILLER, and details of the technique are described by Reed (1997, 1998). SOLVEQ computes the equilibrium distribution of thermodynamic components among aqueous species in the aqueous phase alone, and is used to reconstruct the composition of meteoric water used as an initial fluid in some of the serpentinization simulations. CHILLER computes the equilibrium distribution of components among aqueous species, minerals, and gases, using equilibrium constants for aqueous, solid, and gas reactions at selected temperature and pressure. CHILLER is used to compute reaction paths in geologic systems by changing one of the system variables incrementally, e.g., composition, temperature, pressure, or enthalpy, and re-computing equilibrium at each step. CHILLER and SOLVEQ compute aqueous activity coefficients using the extended Debye-Hückel equation of Helgeson, et al. (1981), as modified by Tanger and Helgeson (1988), and gas fugacities as discussed by Spycher and Reed (1988). The thermodynamic data used by these programs are identical to those described by Palandri and Reed (2001), and are not repeated here. To compute aqueous activity coefficients accu-

Table 1. Mineral abbreviations and formulae.

Abbr	Name	Formula	Abbr	Name	Formula
ab	albite	$NaAlSi_3O_8$	hd	hedenbergite	$CaFeSi_2O_6$
abd	alabandite	MnS	hem	hematite	Fe_2O_3
act	actinolite	$Ca_2Fe_5(Si_8O_{22})OH_2$	hes	hessite	Ag_2Te
Ag	silver	Ag	hz	heazlewoodite	Ni_3S_2
Au	gold	Au	jpt	jaipurite	CoS
ams	amesite	$Mg_4Al_4Si_2O_{10}(OH)_8$	kt	kotulskite	PdTe
and	andradite	$Ca_3Fe_2(SiO_4)_3$	In	linnaeite	Co_3S_4
anh	anhydrite	$CaSO_4$		lizardite	$Mg_3Si_2O_5(OH)_4$
asp	arsenopyrite	FeAsS	mgs	magnesite	$MgCO_3$
atg	antigorite	$Mg_{2.824}Si_2O_5(OH)_{3.647}$	mic	microcline	$KAISi_3O_8$
atg	antigorite	$Mg_{48}Si_{34}O_{85}(OH)_{62}$		minnesotaite	$Fe_3Si_4O_{10}(OH)_2$
	awaruite	γ-NiFe ($Ni_{65-90\%}$)	ml	millerite	NiS
bn	bornite	Cu_5FeS_4	mng	manganosite	MnO
brc	brucite	$Mg(OH)_2$	mt	magnetite	Fe_3O_4
ca	calcite	$CaCO_3$	Ni	nickel	Ni
cam	caminite	$Mg_{1.5}SO_4 \cdot (OH)$	nic	niccolite	NiAs
cc	chalcocite	Cu_2S		Na-nontronite	$Na_{0.33}Fe_2Al_{0.33}Si_{3.67}7O_{10}(OH)_2$
chl-Fe	daphnite	$Fe_5Al_2Si_3O_{10}(OH)_8$	pn	pentlandite	Fe_9S_8
chl-Mg	clinochlore	$Mg_5Al_2Si_3O_{10}(OH)_8$	Co · pn	Co-pentlandite	Co_9S_8
chl-Mn	Mn-chlorite	$Mn_5Al_2Si_3O_{10}(OH)_8$	Pd	Palladium	Pd
chy	chrysotile	$Mg_3Si_2O_5(OH)_4$	PdS	Pd sulfide	PdS
clv	calaverite	$AuTe_2$	por	portlandite	$Ca(OH)_2$
cp	chalcopyrite	$CuFeS_2$	prh	prehnite	$Ca_2Al_2Si_3O_{10}(OH)_2$
ct	cattierite	CoS_2	Pt	platinum	Pt
Cu	copper	Cu	py	pyrite	FeS_2
czo	clinozoisite	$Ca_2Al_3(SiO_4)_3(OH)$	po	pyrrhotite	FeS
di	diopside	$MgCaSi_2O_6$	sp	spinel	$MgAl_2O_4$
dol	dolomite	$CaMg(CO_3)_2$	spr	sperrylite	$PtAs_2$
dsp	diaspore	AIO(OH)		taenite	γ'-NiFe ($Ni_{100-20\%}$)
	electrum	Au-Ag ($Au_{1.00-0.30}$)		talc	$Mg_3Si_4O_{10}(OH)_2$
en	enstatite	$Mg_2Si_2O_6$	tm	tremolite	$Ca_2Mg_5(Si_8O_{22})OH_2$
ep	epidote	$Ca_2(FeAl_2)_3(SiO_4)_3(OH)$	tv	trevorite	$NiFe_2O_4$
Fe	iron	Fe	vsv	vesuvianite	$Ca_{19}Mg_2Al_{11}Si_{18}O_{69}(OH)_9$
fo	forsterite	Mg_2SiO_4		wollastonite	$CaSiO_3$
grs	grossular	$Ca_3Al_2(SiO_4)_3$	wrk	wairakite	$CaAl_2Si_4O_{10} \cdot (OH)_4$

rately, the method requires that NaCl be the dominant solute at ionic strength greater than ~1, and that the total salinity not exceed ~3 molal. Thus we include 5.3 ppm NaCl in the initial rock compositions, so that the former condition is met when using fresh water as the serpentinizing fluid, and we terminate the simulations at ~3.0 molal salinity, which is higher than what is found in most natural waters.

Most of the simulations described herein are water-rock titrations, which allow assessment of the equilibrium distribution of elements over a wide range of water-rock ratios (w/r); we start with a fixed amount of initial fluid, and an arbitrary large amount of fresh rock. Rock is added incrementally to the fluid, and equilibrium is recomputed at each step. At the termination of a simulation, there exists an alteration assemblage and any amount of unreacted fresh rock. In the context of fluid infiltration into veins or fractures and the development of alteration envelopes, results at large w/r show alteration assemblages proximal to a fracture, and at small w/r, distal from a fracture, as explained by Reed (1997). Further, water-rock titrations reveal at large w/r the evolution of fluid composition that may be controlled by the dissolution of primary minerals, as might occur in open fractures. The simulations begin at quite large w/r that may not be attained in natural systems, where alteration minerals are undersaturated and not present. The results illustrate changes that may occur at smaller w/r in natural systems, that may be far from overall equilibrium due to kinetic effects as minerals slowly dissolve. Also recognize that the w/r graphs may be read from right-to-left, for example, to understand the evolution of a process that begins with a small amount of water equilibrating with fresh rock.

In the balanced chemical reactions shown below, an arrow ($\rightarrow$) implies a process that is driven in the indicated direction by an imposed change in system composition, such as titrating rock into water, e.g., reaction (2), below. An equal sign (=) is used to address a state of equilibrium between the reactants and products, e.g., reaction (6). Some reactions are written to address both a unidirectional process and an equilibrium condition, for example chrysotile is both a reaction product and part of a pH buffer equilibrium as in reaction (4); for these cases, the double right arrow symbol ($\Rightarrow$) is used. The phases containing reactants and products are specified in reactions (using abbreviations in Table 1), except that aqueous ionic species are not so identified where it is clear from the context that they are aqueous.

2.1.1. Limitations of the method

Local chemical equilibrium between fluids and alteration minerals is a valid assumption in many volcanic-hosted hydrothermal systems (Arnórsson, 1983; Arnórsson et al., 1983; Giggenbach, 1980, 1981; Pang and Reed, 1998; Reed, 1982, 1997, 1998; Reed and Spycher, 1984), and in many sedimen-

tary systems to temperatures as low as 75–80°C, if fluid flow rates are sufficiently slow (Bazin et al., 1997a, 1997b; Palandri and Reed, 2001). However, it is important to recognize that equilibrium between a fluid and primary minerals is commonly lacking, and in some cases cannot be attained, e.g., forsterite at T and P of H_2O L-V saturation.

Alteration of primary minerals may proceed at different rates; for example, relict pyroxene and spinel may persist in peridotites where olivine has been thoroughly serpentinized (Coleman, 1977). Alteration also commonly leads to precipitation of metastable minerals, e.g., antigorite rather than more-stable chrysotile, during serpentinization. Further, our simulations assume equilibrium between sulfate and sulfide to specify the overall redox state of the system, and this assumption may not always be valid at low temperatures (Giggenbach, 1987, 1993), especially in fluids with low salinity (Stefánsson and Arnórsson, 2002) or high pH (Ohmoto and Lasaga, 1982). These issues are all related to chemical kinetics, and our calculations do not account for absolute rates of mineral dissolution and precipitation, nor of aqueous speciation, which are of increasing importance with decreasing temperature. Nevertheless, the alteration assemblages computed in the simulations, even at temperatures as low as 25°C, show a remarkable similarity to natural alteration assemblages observed in the field. In some cases, relative reaction rates can be simulated by suppressing a more-stable phase where a metastable mineral is expected to precipitate (as for chrysotile and antigorite, discussed below).

Further limitations include: 1) thermodynamic data are absent for a few of the minerals of interest, and in these cases a similar mineral is used as a proxy; 2) if thermodynamic data for endmembers of important solid solutions are present, and solution model data are not, ideality is assumed (further discussion of these first two issues below); 3) many thermodynamic parameters for trace elements used in the simulations are based on empirical correlations and experiments, for which there are a degree of uncertainty, and therefore the results presented with respect to trace elements are best regarded as approximations; 4) The equilibrium constants used are for conditions corresponding to H_2O L-V saturation (but our calculations do not deviate significantly from these conditions); 5) the simulations do not address mineral texture and geometry, such as the size and distribution of alteration minerals grains relative to each other, and relative to primary minerals in partly altered rock.

2.2. The Stability and Selection of Serpentine Phases

Serpentinites are most commonly dominated by lizardite (Aumento and Loubat, 1971; Coulton et al., 1995; Früh-Green et al., 1996; Hébert et al., 1990; Prichard, 1979; Wicks and O'Hanley, 1988). However, thermodynamic data for lizardite are not well constrained experimentally (O'Hanley et al., 1989), and we must therefore select data for either antigorite or chrysotile. O'Hanley et al. (1989) have shown that at near-surface pressures, the reaction

$$\text{chrysotile} \rightarrow \text{brucite} + \text{antigorite} \quad (1)$$

occurs near 250°C, and Evans (1977) suggests the reactant chrysotile forms and persists metastably below that temperature. Our calculations, which rely on thermodynamic data from Holland and Powell (1998), indicate that antigorite is more stable than chrysotile at temperatures from 25 to 350°C, in agreement with Evans (1977). Apparently, chrysotile occurs naturally below 350°C because it is kinetically preferred. To reflect the composition of natural serpentinites, antigorite is suppressed from the calculations at 25°C and chrysotile is forced to precipitate as a proxy for lizardite; at 300°C antigorite is not suppressed. In any case, because free energy change that accompanies serpentinization is large, and because the difference in free energy and chemical composition between the serpentine phases is small, the choice of serpentine phase used in the calculations has only a small effect.

2.3. Initial Fluid and Rock Compositions

Composition data for fresh water and seawater are used for the initial fluid in the simulations (Table 2). The fresh water is the average for rainwater from the West Coast of the United States (Berner and Berner, 1996), and it is assumed to be at equilibrium with atmospheric CO_2 and O_2, with a pH of 5.65 and Eh of 0.88 V. The seawater composition used (Hem, 1985) contains a complete array of minor and trace elements; it has a pH of 8.1, and an arbitrary Eh of −0.22 V. For the rodingitization simulations we used the fluid produced in the simulation of serpentinization with seawater at 300°C at log w/r = 0.4.

An average of eight harzburgites (Coleman, 1977) was used as the starting peridotite composition (Table 3). To reflect accurately the oxidation state of sulfur in fresh harzburgite, sulfur was recomputed as FeS. The amounts of Co, Cl, Cu, As, Ag, Au, Hg, Pd, Pt, and Te in harzburgite are from Wedepohl (1969–1978), and Cl is balanced with Na from Na_2O. To model the formation of rodingite we used two gabbroic rocks with different Al content (Table 3, from Coleman, 1977). One is a pyroxene-bearing gabbro with a composition typical of ophiolite-hosted gabbroic cumulates, and the other is a norite composed mostly of plagioclase and orthopyroxene.

3. SIMPLE MODELS OF SERPENTINIZATION BY FRESH WATER AT 25°C

The chemistry of serpentinization is controlled primarily by six components in the rock: MgO, CaO, SiO_2, Fe_2O_3, FeO, and S. To distinguish how these control various aspects of serpentinization, we simulated three simplified systems at 25°C and 10 bar pressure, in which the rock composition is limited to the six or fewer components. Considered first is a rock composed solely of MgO and SiO_2. Next, CaO is added, and in the third, FeO, Fe_2O_3, and S are added. The initial fluid in all three simulations is meteoric water (Table 2), with K omitted to simplify the problem further.

3.1. The System MgO - SiO_2 - H_2O - CO_2

The fresh rock in this system contains only SiO_2 and MgO (i.e., forsterite and enstatite) in harzburgite (Table 3). Interpretation of the results is made with reference to the solid black curves in Figure 1, and are expressed in terms of chemical changes as a function of the amount of reactant rock added. Figure 1A shows both the protolith and alteration mineral

Table 2. Composition of fluids used in the models, ppm.

	[a]Meteoric water	[b]Seawater	[c]Seawater	[d]Na-Ca-Cl fluid	[e]Na-Ca-Cl fluid
T(°C)	25	25	25	300	160
pH	5.65	8.1	6.97	7.74	8.74
Cl	5.11	18876	18777	20081	20100
[f]SO_4^{-}	2.45	2665	2665	2.0e-08	−1036
HCO_3^{-}	0.80	140	112	81.0	81.0
[f]HS^{-}	—	—	—	125	549
$H_2AsO_3^{-}$	—	0.0049	0.0049	0.017	5.1e-05
H_3BO_3	—	20.9	20.9	22	22
SiO_2	—	6.32	5.55	0.0035	0.00024
Na	3.68	10366	10365	11056	11066
K	0.24	385	385	413	413
Ca	0.58	405	396	1815	1817
Mg	—	1333	1327	0.039	0.036
Al	—	0.001	3.9e-07	40.3	19.8
Fe	—	0.003	0.003	0.047	0.024
Mn	—	0.002	0.002	5.5	—
Ni	—	0.007	0.007	4.4e-07	—
Cu	—	0.003	0.003	0.031	—
Co	—	0.0004	0.0004	7.4e-06	—
Ag	—	0.0003	0.00003	0.017	—
Au	—	0.00001	7.7e-16	0.00028	—
Pt	—	0.000001	5.4e-13	1.5e-14	—
Pd	—	0.000001	5.2e-18	0.0055	—
Hg	—	0.0002	0.0002	0.0019	0.0019

[a] U.S. coastal, average, Berner and Berner, 1996; pH computed from equilibrium with atmospheric CO_2.
[b] Hem, 1985; pH, Berner and Berner, 1996.
[c] Composition of seawater after fractionation of supersaturated clinochlore, dolomite, gold, silver, palladium, quartz and sperrylite.
[d] Fluid product of serpentinization of harzburgite with seawater at 300°C at log w/r = 0.4.
[e] Fluid product of serpentinization of harzburgite with seawater at 300°C at log w/r = 0.4, cooled to 160°C.
[f] Redox state is defined by relative total amounts of HS^{-} and SO_4^{2-}, and therefore negative values are allowed.

assemblages. The protolith minerals forsterite and enstatite are not alteration minerals, and are shown to illustrate their use in a water-rock titration; the amount is arbitrary (~6.0 kg) and slightly in excess of that which can react with 1.0 kg of fluid. Figure 1B shows the fluid composition in terms of components that define the system. Figures 1C–E show the concentrations of important, dominant aqueous species over which the components are distributed, and are useful for examining the distribution of a particular element among aqueous species. For example, the total concentration of Mg is given by the ΣMg curve, and is made up entirely of Mg^{2+}, $MgOH^{+}$, $MgCl^{+}$, and $MgHSiO_3^{+}$; only the first two are shown, as the latter two are less than the ordinate axis minimum in the figure, and Mg^{2+} is dominant at all w/r in the simulation.

Addition of rock to water causes the pH and ΣMg and ΣSiO_2 (i.e., H_4SiO_4) to increase (Figs. 1B,D,E) in accordance with the following forsterite and enstatite dissolution reactions (see Table 1 for mineral name abbreviations):

$$Mg_2SiO_4\ (fo) + 2\ H_2O \rightarrow 2\ Mg^{2+} + SiO_2\ (aq) + 4\ OH^{-} \quad (2)$$

$$MgSiO_3\ (en) + H_2O \rightarrow Mg^{2+} + SiO_2\ (aq) + 2\ OH^{-} \quad (3)$$

The inflection in the pH curve near log w/r = 6.3 results from the titration end point for dissociation of H_2CO_3 to H^{+} and HCO_3^{-} (Fig. 1C). Chrysotile precipitates near log w/r = 5.7 (Fig. 1A), buffering the pH at 9.4. The pH mirrors the total concentration of Mg^{2+} in accordance with the following equilibrium, wherein pH and SiO_2 are weakly buffered by chrysotile:

$$3Mg^{2+} + 2\ SiO_2\ (aq) + 5\ H_2O \Rightarrow Mg_3Si_2O_5\ (OH)_4\ (chy) + 6\ H^{+} \quad (4)$$

The chrysotile buffer begins to fail near log w/r = 5 in response to decreasing aqueous SiO_2 consumed in chrysotile precipitation, and the pH resumes increasing; Mg^{2+} increases because Mg/Si in the protolith is greater than in chrysotile. Brucite precipitates near log w/r = 3.6, buffering the pH at 10.3 and the concentration of Mg^{2+}, by the combined constraints of equilibria (4), (5), and (6). Further OH^{-} and Mg^{2+} produced by dissolution of fresh rock in excess of that removed by chrysotile precipitation, is removed by brucite precipitation:

$$Mg^{2+} + 2\ OH^{-} \Rightarrow Mg(OH)_2\ (brc) \quad (5)$$

Chrysotile and brucite then precipitate in amounts directly proportional to the rock added, and the two minerals buffer the SiO_2 at a low concentration:

$$Mg_3Si_2O_5(OH)_4\ (chy) + H_2O = 3\ Mg(OH)_2\ (brc) + 2\ SiO_2\ (aq) \quad (6)$$

After brucite-in, the fluid composition is nearly constant, affected only by the continuing removal of water by reactions (2), (3), and (4). At the lowest w/r, the dissolved components

Table 3. Compositions of rocks used in the models, weight percent.

	[a]Harzburgite	[b]Gabbro 1 (cpx-opx gabbro)	[c]Gabbro 2 (Eucrite)
olivine	72.6	0.8	4.7
orthopyroxene	23.9	—	—
clinopyroxene	1.7	—	—
spinel	2.3	—	—
plagioclase	—	—	—
orthoclase	—	0.1	0.6
albite	—	3.9	17.0
anorthite	—	52.4	64.0
nepheline	—	—	2.4
diopside	—	22.9	10.9
hypersthene	—	19.6	—
ilmenite	—	0.19	0.2
apatite	—	0.05	—
MgO/(MgO+FeO)	—	0.69	0.56
SiO_2	43.9	48.40	47.40
Al_2O_3	0.94	19.70	27.20
Fe_2O_3	1.34	0.63	0.60
FeO	6.49	3.70	1.80
MgO	45.90	9.40	3.00
CaO	0.60	16.10	15.30
Na_2O	0.0092	0.46	2.50
K_2O	0.0010	0.02	0.10
MnO	0.120	0.10	—
FeS	0.0685	—	—
NiO	0.32	—	—
CoO	0.0130	—	—
NaCl	0.0053	0.0053	0.0053
CuO	0.0059	—	—
As_2O_3	0.00037	—	—
Ag	0.000005	—	—
Au	0.0000007	—	—
Hg	0.0000004	—	—
Pd	0.0000013	—	—
Pt	0.00000032	—	—
Te	0.0000002	—	—
Total	99.71	98.52	97.91

Analyses from, Coleman, 1977.

[a] Burro Mountain, California. Average of 8 samples, analysis #1, page 33; Co, Cl, Cu, As, Ag, Au, Hg, Pd, Pt, Te from the Wedepohl, 1969–1978.

[b] Cyprus, analysis #16, page 43.

[c] Semail Ophiolite, Oman, analysis #14, page 43.

[d] Solid product of serpentinization model with fresh water at 25°C and log w/r = 0.8.

increase sharply, a phenomenon that has been referred to as alteration dry-up (Reed, 1997); at dry-up, >99% of the water has been consumed. The pH is alkaline because there are no magnesium minerals such as chlorite in this aluminum-absent system that are insoluble at neutral pH, thus reactions such as (2) and (3) proceed to produce OH^-.

3.2. The System MgO - SiO_2 - CaO - H_2O - CO_2

The fresh rock in this system contains only SiO_2, MgO, and CaO (Table 3). Interpretation of the results are made with reference to the dashed gray curves in Figure 1. The concentrations of Mg^{2+}, SiO_2, and the pH (Figs. 1B,D,E) are nearly identical to the Ca-free system (above), at w/r larger than brucite precipitation (Fig. 1A). The dissolution of CaO in protolith minerals provides an additional source of OH^-:

$$CaO(ol, px) + 2\ H_2O \rightarrow Ca^{2+} + 2\ OH^- \quad (7)$$

driving the fluid to higher pH, and brucite buffers the pH (Fig. 1B) only over a narrow range of w/r. The higher pH displaces brucite equilibrium toward precipitation, decreasing ΣMg and increasing ΣSiO_2. Calcite precipitates near log w/r = 2.1, a result of the small amount of initial bicarbonate in the fluid. The build-up of Ca^{2+} and OH^- at constant SiO_2 concentration (Figs. 1B,D,E) causes wollastonite to precipitate near log w/r = 1.3:

$$Ca^{2+} + SiO_2\ (aq) + 2\ OH^- \Rightarrow CaSiO_3\ (wo) + H_2O \quad (8)$$

buffering the pH at 12.0; thereafter Mg^{2+} is buffered by brucite equilibrium at constant pH. In natural serpentinites wollastonite is not observed, and Ca must either reside in another mineral, or be removed with the serpentinizing fluid. In terrestrial settings at surface conditions, portlandite is likely to precipitate only as the result of evaporation of $Ca^{2+}-OH^-$ spring water; metastable amorphous $Ca(OH)_2$ gel may also form, later crystallizing into portlandite (Neal and Stanger, 1984). Under conditions of high pH and Ca^{2+} concentration, calcite is quite insoluble and will precipitate if bicarbonate exceeds 10^{-5} m. Ca may be removed with the serpentinizing fluid, and in submarine settings may mix with seawater that provides an ample source of bicarbonate, leading to calcite precipitation in chimneys (Kelley et al., 2001), as explored below. Increased pH may also lead to calcite, magnesite, or dolomite precipitation in tectonically brecciated serpentinites commonly identified as ophicarbonates (Bernoulli and Weissert, 1985; Bonatti et al., 1974; Knipper, 1978; Trommsdorff and Evans, 1977), where the alkaline earth metals may be derived from seawater or seafloor calcareous ooze, in addition to the fluid product of serpentinization.

3.3. The System MgO - SiO_2 - CaO - FeO - Fe_2O_3 - S - H_2O - CO_2

In this system containing SiO_2, MgO, CaO, FeO, Fe_2O_3, and FeS in the reactant rock (Table 3), we examine redox effects that are driven by the oxidation of ferrous iron in the protolith. Sulfur is included to reveal sulfide mineral reactions, that are obscured in more complete simulations (below) that include trace elements. There are small amounts of SO_4^{2-} and HCO_3^- in the initial meteoric water (Table 2); they have a small role in this system, compared to seawater (below) which contains large amounts of both species.

The progression of pH and concentrations of Ca, Mg, and SiO_2 (Fig. 2B), are nearly identical to those in the Fe-S-free system (Section 3.2), at w/r greater than that of andradite precipitation (Fig. 2A). Redox issues aside and considering only pH, the primary difference is that the dissolution of FeO in the protolith provides yet another sink for H^+:

$$FeO\ (ol, px) + H_2O \rightarrow Fe^{2+} + 2\ OH^- \quad (9)$$

allowing the pH to attain larger values, that exceed 14 at alteration dry-up; the initial, final, and buffered pH values are compared in Table 5. The fluid evolves from highly oxidizing

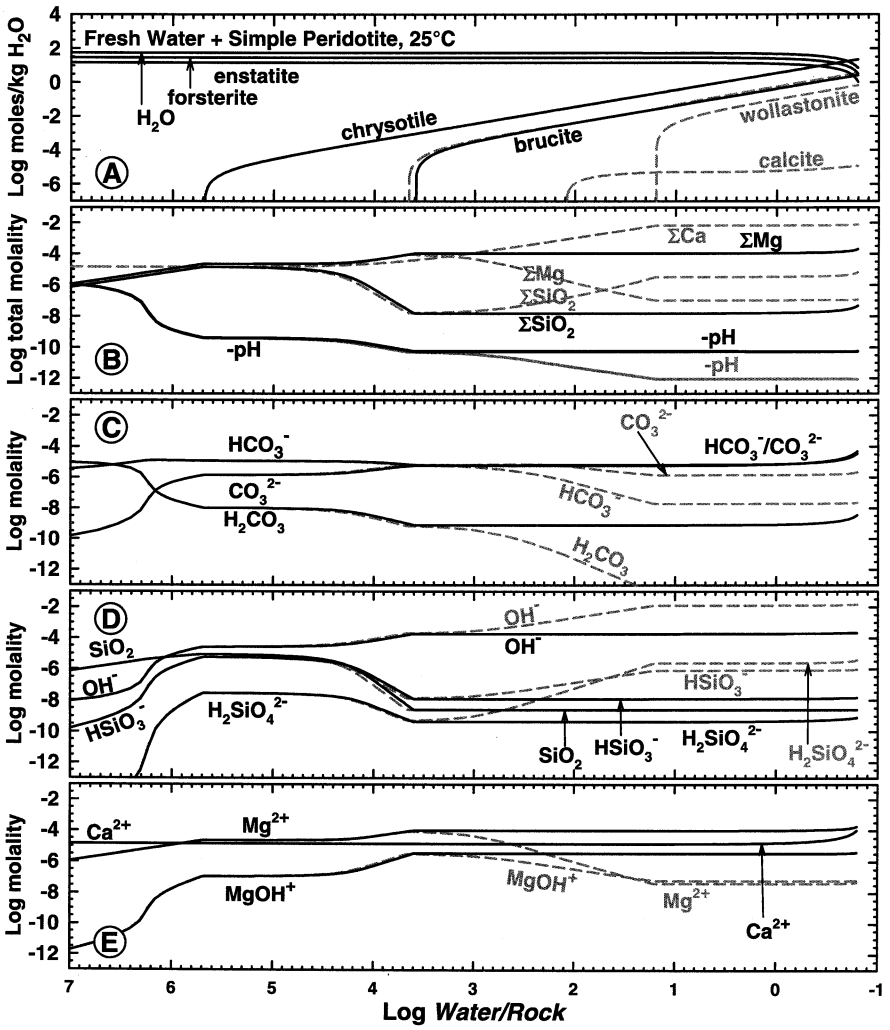

Fig. 1. Serpentinization at 25°C in the systems MgO-SiO_2-H_2O-CO_2 (solid black lines) and CaO-MgO-SiO_2-H_2O-CO_2 (dashed gray lines), equilibrium composition vs. log water/rock (log w/r). A key to the mineral abbreviations is given in Table 1. a) Minerals, log moles per kg of initial fluid. The primary minerals forsterite and enstatite are not part of the equilibrium assemblage. b) Total concentration of aqueous components, molality. c), d), e) Concentration of selected species, molality.

with $f(O_2)$ at an atmospheric level, to highly reducing, dominated by H_2 produced by the reaction:

$$2\ \text{FeO (ol, px)} + H_2O \rightarrow 2\ Fe_2O_3\ \text{(mt, hem)} + H_2 \quad (10)$$

The progression of redox reactions begins with hematite, which forms at the largest w/r considered (off scale left, Fig. 2A). Where pyrite precipitates, hematite, HS^-, and H_2 increase, and Fe^{2+} decreases (Figs. 2C,D), resulting from depletion of H^+, which also drives an increase in hematite:

$$Fe^{2+} + H_2O + 0.125\ SO_4^{2-} \rightarrow 0.5\ Fe_2O_3\ \text{(hem)} + 1.875\ H^+ + 0.125\ HS^- \quad (11)$$

Sulfide from the reactant rock and from sulfate reduction drive initial pyrite precipitation:

$$Fe^{2+} + 0.25\ SO_4^{2-} + 1.75\ HS^- + 0.25\ H^+ \rightarrow FeS_2\ \text{(py)} + H_2O \quad (12)$$

Iron oxidation to form hematite, then magnetite, evolves from balance by reduction of SO_4^{2-} producing HS^- and pyrite, to reduction of HCO_3^- producing CH_4, and finally to reduction of H_2O producing H_2 (Figs. 2C,D,E). In the short w/r interval that hematite and magnetite coexist, the redox potential is buffered at constant pH (buffered by brucite):

$$0.5\ Fe_2O_3\ \text{(hem)} + 0.125\ HS^- \Rightarrow Fe_3O_4\ \text{(mt)} + 0.125\ SO_4^{2-} + 0.125\ H^+ \quad (13)$$

where hematite dissolves out, the redox buffer fails, and sulfur in the fluid changes from sulfate- to sulfide-dominated. Magnetite precipitation drives an increase in H_2 (Eqn. 10), which, with reactant FeO, drives the replacement of pyrite by pyrrhotite:

$$FeS_2\ \text{(py)} + \text{FeO (ol, px)} + H_2 \rightarrow 2\ \text{FeS (po)} + H_2O \quad (14)$$

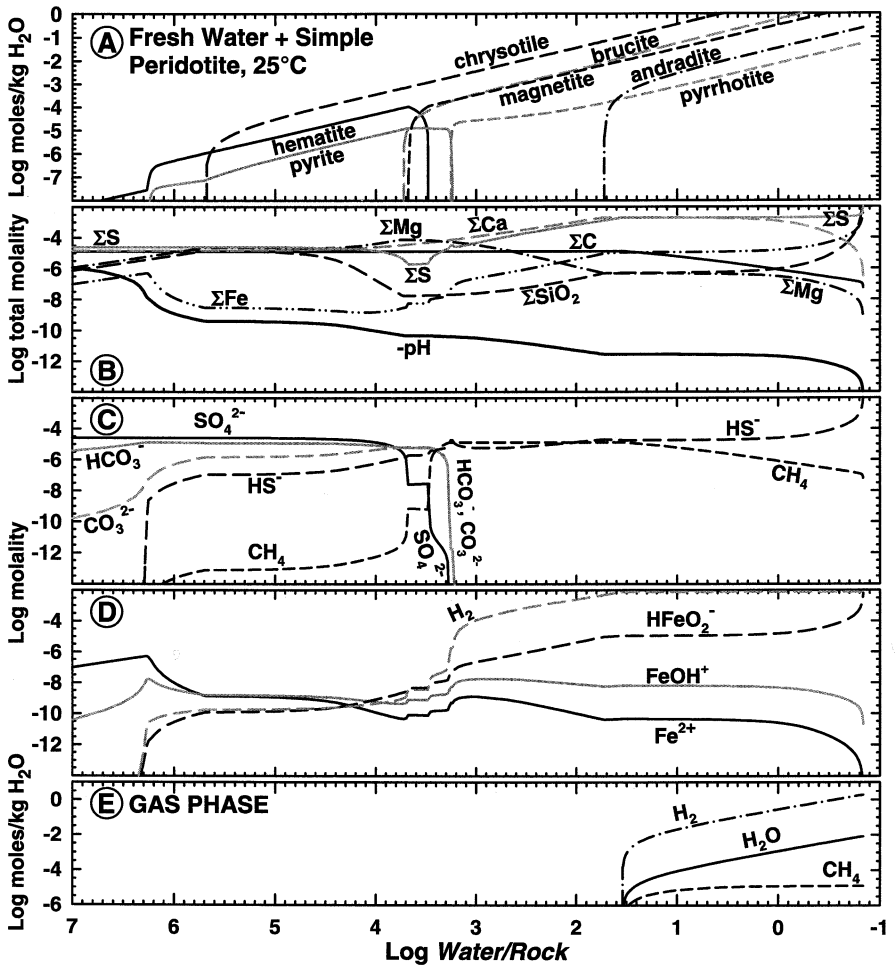

Fig. 2. Serpentinization at 25°C in the system CaO-MgO-SiO_2-FeO-Fe_2O_3-FeS-H_2O(-CO_2), equilibrium composition vs. log w/r. A key to the mineral abbreviations is given in Table 1. a) Minerals, log moles per kg of initial fluid. b) Total concentration of aqueous components, molality. c), d) Concentration of selected species, molality. e) Gas phase composition, log moles per kg of initial fluid.

Andradite precipitates near log w/r = 1.7 and, together with magnetite, large concentrations of Ca^{2+} and H_2, and buffered SiO_2 (Eqn. 6), buffers the pH at 11.6:

$$0.667\ Fe_3O_4\ (mt) + 3\ Ca^{2+} + 3\ SiO_2\ (aq) + 3.667\ H_2O = Ca_3Fe_2Si_3O_{12}\ (and) + 0.667\ H_2\ (g) + H^+ \quad (15)$$

The pH buffer fails as Ca^{2+} is depleted by andradite precipitation, and further increase in pH drives a decrease in Mg^{2+} and Ca^{2+}, as necessary to maintain equilibrium with brucite and andradite; here the Fe^{2+} concentration reaches a level sufficient to balance additional OH^-.

The production of a gas phase at P = 10 bar (Fig. 2E), is another feature absent in the simpler systems. The gas is more than 99.5 mol. % H_2, with minor H_2O and CH_4, and results from reduction of H in water and C in bicarbonate, driven by oxidation of ferrous Fe:

$$3\ FeO\ (ol, px) + H_2O \rightarrow Fe_3O_4\ (mt) + H_2(g) \quad (16)$$

$$12\ FeO\ (ol, px) + HCO_3^- + H^+ + H_2O \rightarrow 4\ Fe_3O_4\ (mt) + CH_4\ (g) \quad (17)$$

The fraction of CH_4 decreases with decreasing w/r because it is limited by the amount of HCO_3^- in the initial fluid. The redox potential in volts is initially 0.88, −0.26 at pyrite-in, then −0.36 at chrysotile-in, −0.45 at magnetite-in, −0.56 at pyrrhotite-in, −0.71 at andradite-in, and −0.87 near alteration dry-up.

In summary, serpentinization is driven by the instability of olivine and pyroxene in water. Mafic mineral dissolution drives the fluid to hyperalkalinity, and oxidation of ferrous Fe drives the system to be highly reducing. In Ca- and Fe-free systems, serpentine weakly buffers the pH at 9.4. The pH is higher if Ca (or Fe) is present, displacing Mg to brucite precipitation, leading to Ca^{2+}-OH^- dominated fluid. At large w/r the system is oxidizing and hematite is stable; with decreasing w/r the system is reduced, and hematite is replaced by magnetite. Oxidation of Fe reduces H in water, producing H_2, and reduces C in HCO_3^- producing CH_4. This process produces the H_2 and light hydrocarbon gases observed in some terrestrial hyperalkaline springs (Abrajano et al., 1990; Coveney et al., 1987; Neal and Stanger, 1983), and in submarine serpentinization (Bougault et al., 1993; Charlou et al., 1991; Charlou and Donval, 1993; Holm and

Charlou, 2001; Rona et al., 1992). An essential feature of this system is that the brucite-chrysotile pair buffers aqueous SiO_2 at such a small activity that no ferrous iron silicates precipitate, leaving magnetite as the most stable alternative repository for Fe.

4. SERPENTINIZATION OF HARZBURGITE

The following addresses a more complete chemical system, including minor NiO, MnO, and Al_2O_3, and trace Na_2O, K_2O, CoO, CuO, As_2O_3, Ag, Au, Hg, Pd, Pt, and Te in peridotite (Table 3). These elements allow for computation of several solid solutions, native nickel or taenite (Ni, Fe), chlorite (Mg, Fe^{II}, Mn), garnet ($CaFe^{III}$, CaAl), and magnetite (Fe^{II}, Ni), all assumed to be ideal, and electrum (Ag, Au). Because thermodynamic data for some mineral endmembers are absent, some solid solutions which may be significant in natural systems cannot be computed; these include Fe, Mn, and Al in brucite, and Ni, Al, Fe, and Mn in serpentine. The high-temperature (>350°C) phase taenite (NiFe) is used as a proxy for awaruite (Ni_3Fe) because awaruite thermodynamic data is absent.

The dominant rock components impose a similarity between these systems and the simplified simulations, with respect to the pH buffers and the strong reduction effect. The following discussion therefore focuses on differences resulting from including minor and trace elements, and further reference herein to "the simple system" refers to the system MgO-CaO-SiO_2-FeO-Fe_2O_3-S-H_2O (Section 3.3).

4.1. Serpentinization of Harzburgite by Fresh Water at 25°C

Presence of Al results in the precipitation of two aluminous phases (Fig. 3A). Diaspore precipitates near log w/r = 8.1, that is replaced by chlorite which persists until alteration dry-up. The composition of chlorite (Fig. 3B) is strongly dominated by the magnesian endmember chlinochlore, and chlorite is the only Mn-bearing mineral that occurs. Aluminum in natural serpentinites may also reside serpentine, and in relict pyroxene and spinel (Coleman, 1977).

The dominant metal in sulfide minerals is nickel, rather than iron as in the simple system. Nickel occurs in millerite, pentlandite, heazlewoodite, niccolite, and taenite, and as trevorite in solid solution with magnetite (Fig. 3A; see Table 1 for mineral formulae). There is a general trend with decreasing w/r such that the dominant sulfide mineral is replaced by another with a larger ratio of metal to sulfide. In the simple system pyrite is replaced by pyrrhotite; here, pyrite and millerite are replaced by heazlewoodite. Where hematite dissolves (log w/r = 3.4, Fig. 3A), aqueous H_2 increases sharply (Fig. 3D), driving the Ni-sulfide replacement reaction analogous to that for iron in reaction (14):

$$NiS_2\ (mil) + 2NiO\ (ol, tv) + 2\ H_2 \rightarrow Ni_3S_2\ (hz) + 2\ H_2O \quad (18)$$

The sequence of Fe- and Ni-sulfides starts with pyrite and millerite; pentlandite replaces pyrite shortly after hematite dissolves out, followed by the replacement of millerite by heazlewoodite. The composition of magnetite varies, but never exceeds 2.5 wt % trevorite. Despite the absence of thermodynamic data for awaruite and its consequent exclusion from the calculations, it is clear that conditions attained are sufficiently reducing to precipitate native nickel-iron alloy.

Dissolved arsenic increases (Figs. 3I,J until niccolite precipitates (Fig. 3G), and at smaller w/r arsenic is exceedingly insoluble. Mercury does not occur in minerals, and exists in solution primarily as Hg° (Fig. 3J); at alteration dry-up its concentration is 0.017 ppm. The elements Co, Cu, Ag, Au, Te, Pt, and Pd reside only in minerals containing these native metals, sulfur, and arsenic. The replacement sequence of cobalt minerals is ct-ln-Co · pn (Fig. 3G). There is a trend of increasing Co/S, caused by decreasing redox potential and production of H_2, driving reactions analogous to (14) and (18). For copper, the sequence is Cu-cc-cp-bn-Cu (Fig. 3G). There is an initial trend of decreasing Cu/S until bornite-in, driven by the increased availability of sulfur from the fresh rock. The trend reverses at bornite-out, driven by decreasing redox potential and H_2 as for the Ni- and Co-sulfides.

Gold, silver and tellurium are chemically linked because they form compounds only with each other (electrum and hessite, Fig. 3H), and their aqueous concentrations are small. Platinum and palladium also show low solubility (Figs. 3I,J), and both form as native metals with the first increment of added fresh rock; they dissolve out before precipitation of sperrylite ($PtAs_2$) and PdS (Fig. 3H), the latter replaced by native Pd near log w/r = 3.2. Low solubility of Ag, Au, Te, Pd and Pt and their precipitation at large w/r show that they are not mobilized, and therefore their spatial re-distribution upon rock alteration is likely to be small. There is a decrease in the solubility of trace metals at 25°C with increasingly reducing conditions, except for Hg, Te, and Co. Serpentinization by fresh water at 100°C (not shown in figures) is not substantially different from that at 25°C.

4.2. Serpentinization of Harzburgite by Seawater at 300°C

Seawater-harzburgite simulations were computed at 25, 100 (P = 10 bar; not shown in figures) and 300°C (P = 100 bar). At small w/r the mineral products at 25 and 100°C in seawater and meteoric water are all quite similar. Differences include: substantial HCO_3^- and SO_4^{2-} present in the initial seawater buffer and shift the pH increase and the strong reduction effect to much smaller w/r than for meteoric water, and result in carbonate and sulfate mineral precipitation at relatively large w/r; at small w/r the carbonate is reduced, leading to larger amounts of CH_4. Less significant differences result from the presence of Na^+, Mg^{2+}, and SiO_2 in seawater, which precipitate in Na-nontronite and talc at large w/r. At small w/r, the differences fade because the chemistry of both systems is dominated by rock.

Serpentinization by seawater at 300°C is substantially different from the lower temperature simulations, in part because the serpentine phase is antigorite (Fig. 4A) rather than chrysotile, as antigorite is not suppressed as explained above. However, most of the differences result from the higher temperature rather than the choice of serpentine phase. Caminite precipitates with the first increment of rock added (off scale left, Fig. 4B), and with high concentrations of Mg^{2+} and SO_4^{2-} (Figs. 4C,E), buffers the pH at 5.2:

$$1.5\ Mg^{2+} + H_2O + SO_4^{2-} \Rightarrow Mg_{1.5}SO_4\ (OH)(cam) + H^+ \quad (19)$$

Dissolution of fresh rock drives the reaction by consuming H^+, until the increasing pH leads to brucite precipitation (Fig. 4A), buffering the pH near 5.4 as in reaction (5). Anhydrite replaces caminite (Fig. 4B) because Mg^{2+} is displaced to brucite, and Ca^{2+} increases from the added fresh rock. Anhydrite dissolves out because sulfate is consumed in reduction to sulfide (Fig. 4E). Aqueous Mg^{2+} is depleted near log w/r = 1 (Fig. 4C) in response to antigorite and brucite precipitation, and the brucite pH buffer fails. Where portlandite precipitates the pH is buffered at 7.8 in a reaction analogous to brucite (Eqn. 5).

There are four redox buffers at 300°C. First is the hematite-magnetite buffer (Eqn. 13), that operates until hematite dissolves out, but only after magnetite activity in solid solution becomes large relative to trevorite. Second is the magnetite-pyrite-pyrrhotite buffer that exists over the short interval of coexisting pyrite and pyrrhotite:

$$3\ FeS_2\ (py) + 4\ H_2 + Fe_3O_4\ (mt) = 6\ FeS\ (po) + 4\ H_2O \quad (20)$$

The third redox buffer is the magnetite-pyrrhotite buffer that operates in conjunction with pH buffered by portlandite, between portlandite-in and pyrrhotite-out:

$$FeS\ (po) + 3H_2O + 0.25\ SO_4^{2-} = Fe_3O_4\ (mt) + 2.75\ H^+ + 3.25\ HS^- \quad (21)$$

Finally, coexistence of alabandite and manganosite (Figs. 4A,B), with pH buffered by portlandite, buffers redox from manganosite-in near log w/r = −0.2 to alteration dry-up:

$$MnO\ (mng) + H^+ + HS^- = MnS\ (abd) + H_2O \quad (22)$$

Computed precipitation of manganese phases may reflect the lack of thermodynamic data for solid solution of manganese in serpentine and brucite.

The initial seawater radically changes composition (Figs. 4C–E,H–J), and results at 300°C sharply depart from those at lower temperature. Most prominent is that the Al concentration increases by more than six orders of magnitude (Fig. 4D), exceeding 30 ppm at w/r <0.5, because aqueous $NaAlO_2$ forms at high pH and high temperature. Ca and HS^- increase by three orders of magnitude, and Mg decreases by four orders of magnitude.

Most transition metals are held in alteration minerals, but Au, Ag, Pd, and Pt (Fig. 4H) are enriched in the aqueous phase. Fe and Ni reside mostly in hematite and magnetite-trevorite. With decreasing w/r, the sequence of Co-bearing minerals is ct-ln-jpt (Fig. 4G), and for Cu-bearing minerals, bn-cp-bn (Fig. 4G). Total aqueous Co and Cu reach maxima in the range of 10^{-6} m (Fig. 4H,I) before they are limited by sulfide precipitation (Fig. 4G); these concentrations are small relative to the total amount available, and relative to the concentrations necessary for forming ore deposits. In contrast, Au, Ag, Pd and Pt reach maxima at much smaller w/r than Co and Cu, meaning a larger mass of harzburgite is leached before the precious metals are fixed in the altered rock as native elements, arsenides, or tellurides (Fig. 4G). Their concentration maxima are in the range that produces ore deposits: Ag, 1.86 ppm; Au, 1.7 ppb; Pd, 22 ppb; Pt, 6.4 ppb (Fig. 4H). These metals are held in bisulfide complexes (Fig. 4J), as bisulfide concentrations are large because of the complete reduction of sulfate to sulfide. The sulfide depresses Cu and Co, which form sulfide minerals, but it enhances precious metal concentrations. The dissolved amounts of precious metals depend on pH and the availability of sulfide to form complexes, but pH is a more significant factor in the solubilities of Au and Pt than in the solubilities of Ag and Pd. No mercury minerals precipitate, and the smaller amount of dissolved Hg (1.5 ppb, Figs. 4H,I) than at 25°C can be attributed a larger amount of mercury escaping into the gas phase (off-scale low, Fig. 4F) at higher temperature.

4.3. Comparison of Computed Results to Natural Systems

Computed serpentinization mineral assemblages at small w/r are similar to natural assemblages, despite large differences in the initial fluid compositions. In the simulations at all temperatures considered, serpentine is dominant, making up over 80 wt. % of the mineral assemblage at log w/r <5.0 in fresh water, and at log w/r <3.5 in seawater. At smaller w/r, the computed assemblages all contain magnetite and brucite, and as the aluminous phase either chlorite or amesite, all between 4.0 and 10.0 wt. %. Either magnetite or hematite occurs at log w/r <4.0, with magnetite always replacing hematite with decreasing w/r as the systems become more reducing; the replacement is delayed to lower w/r in seawater because of buffering against reduction by bicarbonate and sulfate. Serpentine ± magnetite has been reported by many authors, in both submarine (Aumento and Loubat, 1971; Früh-Green et al., 1996; Hébert et al., 1990; Mével and Stamoudi, 1996; Rona et al., 1987; Schandl and Gorton, 1995), and terrestrial systems (Coleman, 1977; O'Hanley, 1996; O'Hanley and Dyar, 1993), some of which may have been serpentinized in marine environments. In studies that include many samples, presence of brucite (Aumento and Loubat, 1971; Früh-Green et al., 1996; O'Hanley, 1996; O'Hanley and Dyar, 1993; Rona et al., 1987) and talc (Aumento and Loubat, 1971; Früh-Green et al., 1996; Hébert et al., 1990; Schandl and Gorton, 1995) are variable. Absence of brucite and presence of talc may be attributed to removal of Mg by the fluid, or to protoliths with more pyroxene relative to olivine, or to silica addition from some other source, e.g., seawater at high w/r. Brucite may also result from metamorphic processes such as reaction (1) (Evans, 1977; O'Hanley et al., 1989). Hematite with and without magnetite, are also reported (Aumento and Loubat, 1971; Schandl and Gorton, 1995). The occurrence of hematite and magnetite together may be indicative of late oxidation of magnetite, high temperature alteration, or a lower temperature equilibrium over the narrow range of w/r indicated in the simulations. Chlorite is reported as alteration rinds on spinel (Früh-Green et al., 1996; Hébert et al., 1990), in accordance with the low solubility and mobility of aluminum.

Differences from natural serpentinites include the precipitation of the Ca- and Al-bearing minerals portlandite and amesite at 300°C, and andradite at the lower temperatures. Given that antigorite may contain on the order of 1.0 wt. % Al_2O_3, (e.g., Deer et al., 1992; Ulmer and Trommsdorff, 1995), and that solid solution extends from lizardite to amesite (Chernosky et al., 1988; Wicks and O'Hanley, 1988), natural serpentinization

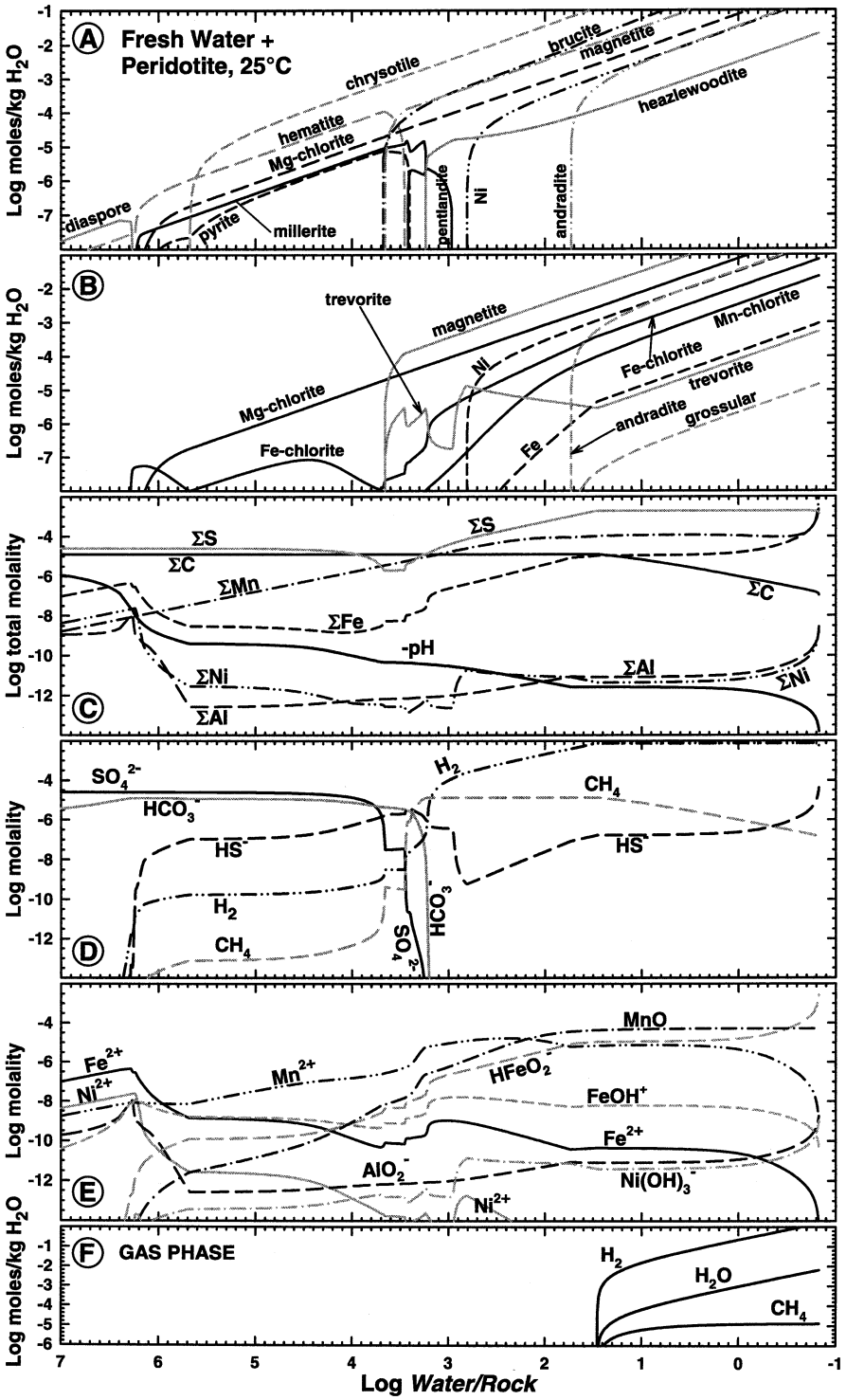

Fig. 3. Serpentinization at 25°C of harzburgite (Table 3) by meteoric water (Table 2), equilibrium composition vs. log w/r. A key to the mineral abbreviations is given in Table 1. a) Major and selected minor minerals. b) Solid solution compositions as endmembers. c) Total concentration of aqueous components. Ca and Mg are nearly identical to those in Fig. 2, and are omitted here for clarity. d), e) Concentration of selected species. f) Gas phase. g) Trace minerals and selected minor minerals. h) Trace minerals. i) Total concentration of trace aqueous components. j) Concentration of selected trace species.

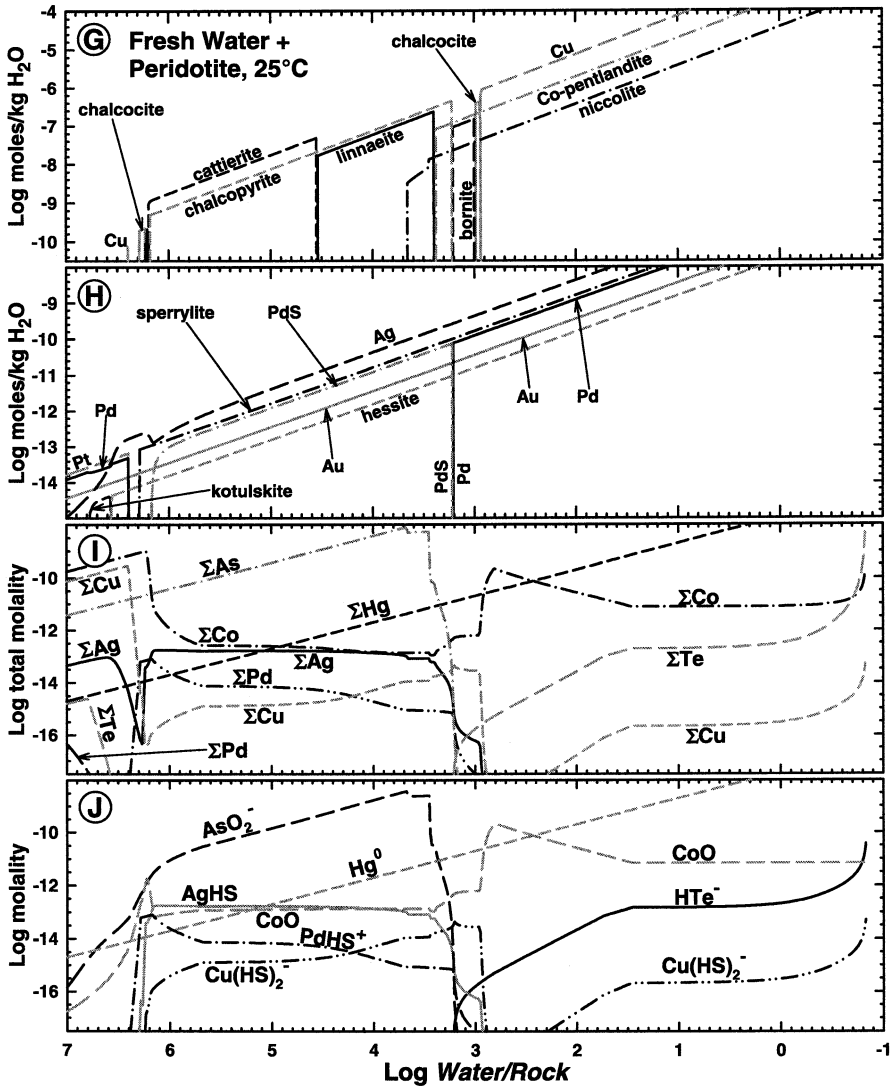

Fig. 3. (Continued)

at 300°C likely results in precipitation of chlorite or aluminous antigorite or lizardite, rather than in amesite. It is unclear why portlandite is computed at 300°C, instead of andradite that precipitates at lower temperatures, especially considering the occurrence of andradite in josephinites (Botto and Morrison, 1976; Frost, 1985). A possible explanation is that the portlandite thermodynamic data (Wolery, 1992) are at the limit of their valid temperature range, and may be inconsistent with the andradite data of Holland and Powell (1998).

Various combinations of many native metals and sulfide minerals have been reported in natural serpentinites, including awaruite, taenite, marcasite, pyrite, pyrrhotite, copper, chalcopyrite, bornite, covellite, heazlewoodite, millerite, pentlandite, valleriite, and violarite (Abrajano and Pasteris, 1989; Alt and Shanks, 1998; Botto and Morrison, 1976; Eckstrand, 1975; Frost, 1985; Lorand, 1987; O'Hanley and Dyar, 1993), of which pyrrhotite, pentlandite, and chalcopyrite may occur as primary minerals (Alt and Shanks, 1998; O'Hanley, 1996). Filippidis (1985) has shown experimentally that serpentinization of Mg-Fe-Ni olivine at 350°C produces awaruite, magnetite, and heazlewoodite. Alt and Shanks (1998) suggest that low $f(O_2)$, low sulfur assemblages containing Ni-Fe alloys, pentlandite, and heazlewoodite are the result of oxidation of ferrous iron to magnetite at small w/r, and that high $f(O_2)$, high sulfur assemblages containing hematite, pyrite, millerite, valleriite, ± magnetite, result from nearly complete oxidation of iron at high w/r. These assemblages are in good agreement with those we have computed: magnetite, native metals and alloys, and either pyrrhotite or heazlewoodite at low w/r, compared with hematite, pyrite, and millerite at high w/r. Although sulfide in some natural assemblages is depleted in ^{34}S as a result of microbial sulfate reduction (Alt and Shanks, 1998), the simulations indicate that biologic activity may not be required to produce the observed minerals.

Computed and natural fluid compositions also show a high degree of similarity with respect to major elements. Table 4 shows compositions of some waters produced by serpentinization computed herein, compared with natural spring waters

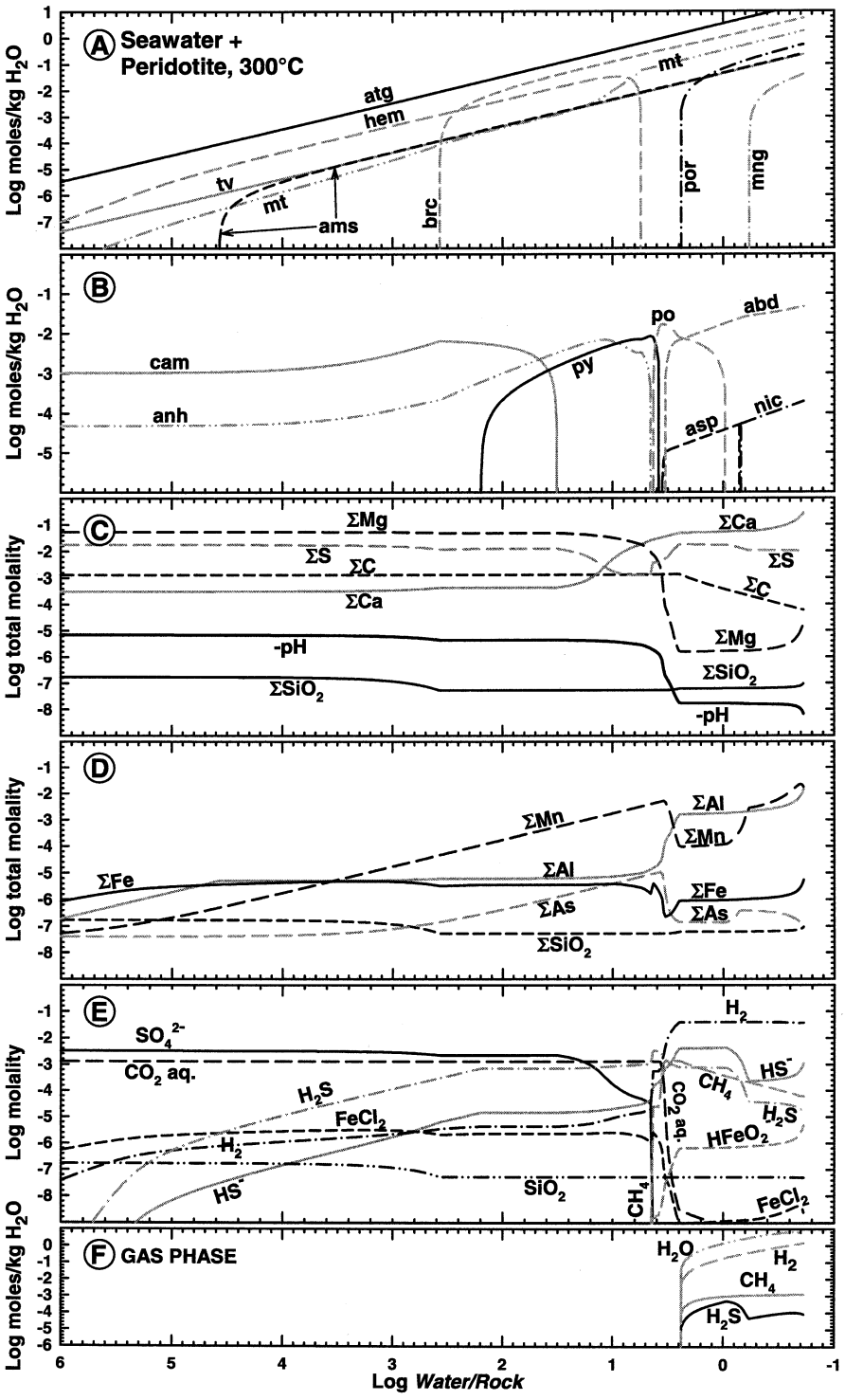

Fig. 4. Serpentinization at 300°C of harzburgite (Table 3) by seawater (Table 2), equilibrium composition vs. log w/r. A key to the mineral abbreviations is given in Table 1. a), b) Major and selected minor minerals. c), d) Total concentration of aqueous components. e) Concentration of selected species. f) Gas phase. g) Trace and selected minor minerals. h) Total concentration of trace and minor aqueous components. i), j) Concentration of selected trace and minor species.

from serpentinites (Barnes and O'Neil, 1969, 1971; Barnes et al., 1978). All show high pH and are enriched in Ca, and show low concentrations of Mg, Fe, silica, bicarbonate, sulfate, and sulfide.

Serpentinization commonly leads to conditions sufficiently reducing to produce H_2 and CH_4. In submarine environments CH_4 occurs in hydrothermal plumes, some examples of which have been attributed to serpentinization (Bougault et al., 1993;

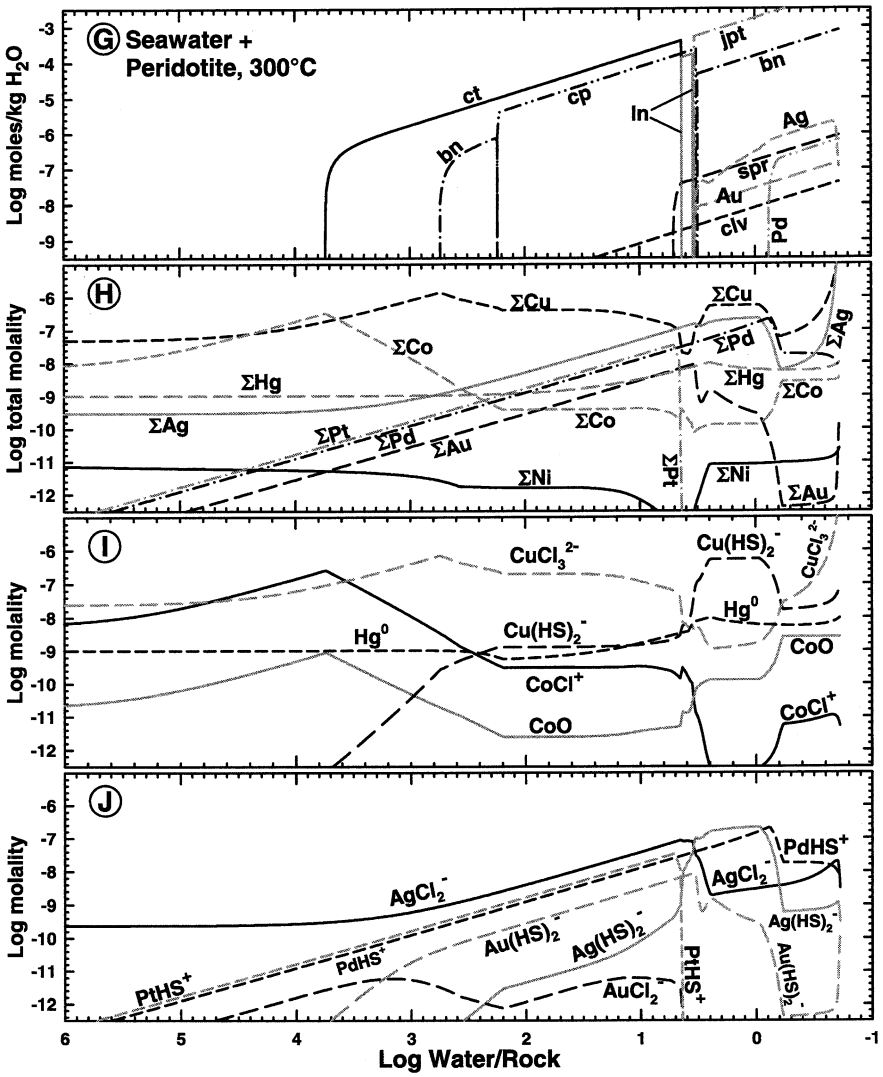

Fig. 4. (Continued)

Charlou et al., 1991; Charlou and Donval, 1993; Holm and Charlou, 2001; Rona et al., 1992). In continental settings, mixtures of H_2, CH_4, and light hydrocarbons issue from hyperalkaline springs (Neal and Stanger, 1983), or from seeps and drill holes in ultramafic bodies (Abrajano et al., 1988; Coveney et al., 1987; Neal and Stanger, 1983). It is generally agreed that H_2 is produced by reduction of water by oxidation of ferrous iron (Eqn. 16) during serpentinization (Abrajano et al., 1988, 1990; Berndt et al., 1996; Coveney et al., 1987; Holm and Charlou, 2001; McCollom and Seewald, 2001; Neal and Stanger, 1983). Less certain is the source of carbon that combines with H_2 to produce CH_4 and other hydrocarbons. One hypothesis is that the carbon is derived from seawater bicarbonate (Abrajano et al., 1988, 1990; Berndt et al., 1996; Charlou et al., 1998; Charlou and Donval, 1993; Kelley and Früh-Green, 1999). Alternatively, CH_4 may be derived from mantle C in fresh olivine (McCollom and Seewald, 2001). In any case, ferrous Fe in primary silicates is the strong reducing agent necessary to produce H_2, and serpentinized rocks contain significantly greater amounts of ferric Fe (in magnetite) and lesser amounts of ferrous Fe than the fresh ultramafic rock, clearly showing that Fe is oxidized in serpentinization (Abrajano et al., 1988, 1990; Alt and Shanks, 1998; Berndt et al., 1996; Coleman, 1977; Coveney et al., 1987; McCollom and Seewald, 2001; Neal and Stanger, 1983).

The computed serpentinite density is ~2.7 g/cm^3 at w/r less than that at which magnetite precipitates. Using an assumed fresh rock density of 3.3 g/cm^3, the volume increase is ~40%. The volume change depends critically upon the relative amounts of olivine and pyroxene, and the amount of Fe in the fresh rock. Our results agree with those of Hostetler et al. (1966), who calculated volume increases between 26 and 50%, for serpentinites of various compositions. The large volume increase immediately raises the question of how strain in the rock is accommodated, especially in consideration of the pseudomorphism and preservation of protolith textures commonly observed in serpentinites. This issue has been addressed by a number of workers, and their work is summarized by

Table 4. Comparison of Ca^{2+}-OH^- spring waters to fluid product of serpentinization by meteoric water, mg/L.

Sample	John Day Warm Spring	Cazadero A	Hahwalah	La Coulée 2	Computed reacted meteoric waters at 25°C	
Location	Grant Co., Oregon, U.S.A.	Sonoma Co., California, U.S.A.	Wadi Jizi, Oman	New Caledonia	log w/r = 3	log w/r = 1
pH	11.25	11.77	11.5	10.7	10.52	11.58
T °C	31	18	25	23	25	25
Ca^{2+}	35	53	60	10.8	4.7	78.6
Mg^{2+}	0.1	0.3	0.1	5.9	0.76	0.011
Na^+	33	50	230	26.1	3.8	12.7
K^+	2.3	1.2	8	3.3	0.24	1.09
Cl^-	19	55	280	16.3	5.1	8.4
SO_4^{2-}	0	0	9	5.8	1.0e-26	1.8e-33
HCO_3^-	0	0	0	0	0.80	0.43
Fe^{2+}	—	0.01	—	—	0.014	0.64
Mn^{2+}	0.01	0.05	—	—	0.92	6.36
Al^{3+}	0.7	0	—	—	2.6e-08	2.0
H_2S	0.4	NA	—	—	3.8e-07	1.7e-07
SiO_2	5.9	0.3	0.4	2.8	0.0016	0.032
OH^-	50.5	62.3	—	—	6.0	71.4
NH_3	0.2	0.1	—	—	—	—
B	0.1	0.01	0.02	—	—	—

O'Hanley (1996): Differential strain between fresh protolith and serpentinite is accommodated by fracturing at scales from microscopic to macroscopic. In brittle material, differential strain requires open fractures, but in serpentine that can deform plastically, the cracks are closed by lithostatic pressure. Ultimately, the textures are preserved, although mineral pseudomorphs are larger than fresh mineral grains in the protolith. At the largest scales, fractures are manifested as cataclastites and shear zones, and the protolith textures are not preserved.

It has been shown experimentally that serpentinite has permeability comparable to shale, so that serpentinizing fluids move primarily by diffusion at the scale of serpentine mineral grains, and fractures are not required for serpentinization to proceed (Macdonald and Fyfe, 1985). Apparently, volume expansion can inhibit serpentinization by sealing fractures and inhibiting fluid flow (Schroeder et al., 2002), or by increasing the free energy of the reaction due to increasing pressure, but volume expansion cannot completely inhibit fluid influx.

It is instructive to compare the results of seawater reaction with peridotite to reaction with basalt at 300°C (e.g., Reed, 1983). The most conspicuous difference is that whereas pH *increases* from nearly neutral in the peridotite reaction, pH *decreases* from neutral (5.5, 300°C) to quite acidic values (e.g., 3.8) in the basalt reaction. The pH decrease in the basalt reaction results from precipitation of chlorite, drawing Al from the basalt and Mg^{2+} from the seawater (Reed, 1983; Seyfried and Mottl, 1982). In the peridotite reaction, the lack of aluminum precludes forming a stable Mg-Al-silicate that would produce sufficient H^+ to overwhelm the caminite and brucite buffers. This difference in pH leads to the difference between the basalt and peridotite systems in transport of base metals at large w/r. The acidic basaltic-derived fluid leaches and mobilizes base metals despite substantial concentration of aqueous sulfide. In contrast, the neutral to alkaline, peridotite-derived fluid allows sulfide minerals to form, removing base metals from solution.

5. SEA FLOOR CARBONATE CHIMNEY PRECIPITATION

Submarine hydrothermal vents discharging fluid products of serpentinization on the Mid-Atlantic Ridge precipitate calcite, aragonite, and brucite, upon mixing with seawater (Kelley et al., 2001). The vent fluids are alkaline, enriched in Ca, and depleted of Mg and sulfate relative to seawater (Kelley et al., 2001), as we have computed above. When mixed with cold seawater, the alkaline vent fluid drives the calcite precipitation reaction (Kelley et al., 2001):

$$Ca^{2+} + HCO_3^- + OH^- \rightarrow CaCO_3(s) + H_2O \qquad (23)$$

Concentrated hydroxide also drives brucite precipitation, reaction (5), with Mg derived from seawater.

The computed reaction begins with cooling of serpentinization fluid obtained at log w/r = 0.4 at 300°C (Table 2). The fluid is cooled, as might occur in the conduit as the fluid ascends from its source rocks, to 160°C. This temperature is significantly higher than the 40 to 70°C reported by Kelley et al. (2001), and was selected because mixing with only a small amount of cold seawater leads to the observed temperatures (Fig. 5C). Pressure is constant at 100 bar, and trace elements are omitted for simplicity. In this system, heat is likely derived from exothermic serpentinization, rather than a volcanic source (Kelley et al., 2001). The hot spring fluid is mixed with cold seawater at 4°C, in ratios (cold seawater to hot spring fluid, referred to as c/h, below) from 0 to 50 by weight.

Brucite precipitates with the first 0.001 kg increment of added seawater (Fig. 5A), with lesser amounts of diaspore, amesite and pyrrhotite. The pH decreases sharply and Mg increases (Fig. 5B) until the brucite buffer, reaction (5), takes effect near c/h = 0.1. The buffer persists until brucite-out near c/h = 6.6; the pH increase in this interval is due to cooling, in combination with the temperature dependence of the brucite stability constant. With further mixing, the pH resumes decreasing, approaching that of cold seawater at the largest c/h. Calcite precipitates near c/h = 0.3, and magnesite precipitates

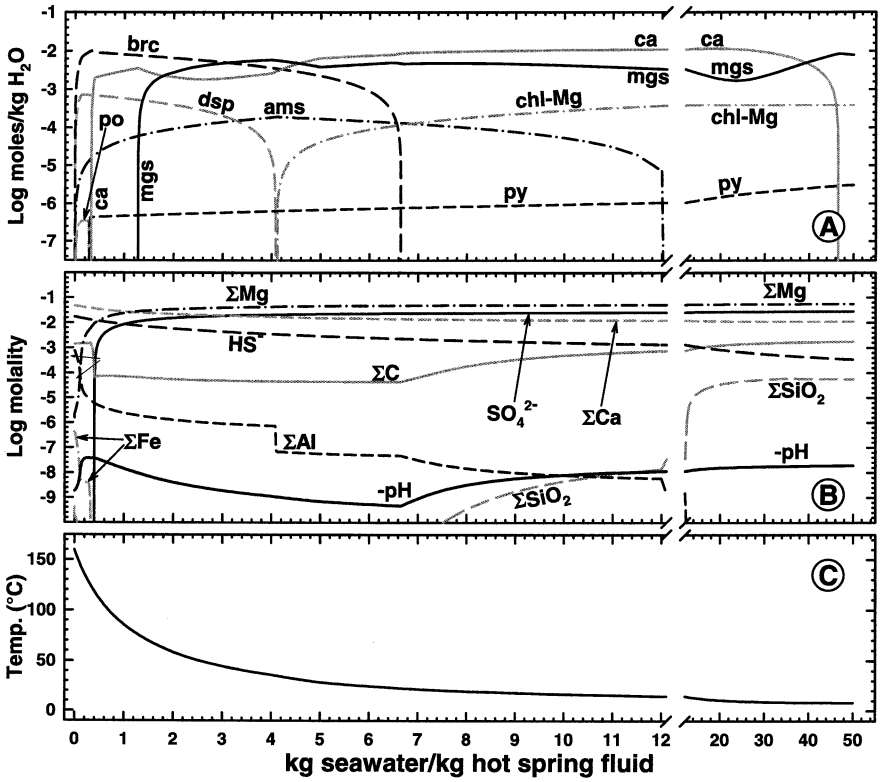

Fig. 5. Mixing of the 300°C fluid product of serpentinization at log w/r = 0.4 (Table 2), cooled to 160°C, with cold seawater at 4°C, equilibrium composition vs. ratio of cold seawater to hot spring fluid in kg. A key to the mineral abbreviations is given in Table 1. a) Minerals. b) Concentration of aqueous components except sulfur. c) Fluid temperature.

near c/h = 1.3. Magnesite is the dominant mineral precipitate between c/h = 3 to 5, and c/h greater than ~40; calcite dominates from c/h = 5 to 38. The Ca in calcite is derived primarily from the vent fluid, because the cold seawater serves only to dilute the high concentration of Ca in the initial hot fluid (Fig. 5B); Mg in magnesite is derived primarily from cold seawater, as the initial vent fluid contains negligible Mg. Bicarbonate is derived mostly from cold seawater, with a small amount initially derived from oxidation of CH_4 in the vent fluid. In this calculation, both calcite and magnesite are metastable with respect to dolomite, which is disallowed because we expect it to precipitate more slowly, owing to the higher degree of ordering in its structure (Helgeson et al., 1978).

An additional mixing reaction simulation (not shown in figures) using the 300°C fluid without first cooling it, results in a carbonate assemblage dominated by magnesite; calcite exists only over a short interval between c/h = 0.2 and 0.4, and is replaced by magnesite that persists to c/h >50. Cooling is assumed to have a conductive component as the fluid ascends through a conduit, and as it flows and diffuses though the carbonate pile. The two mixing reactions simulate mixing, and a combination of cooling and mixing, and the relative amounts of calcite and magnesite may depend critically upon the relative amounts of cooling by conduction and mixing, as well as the kinetics of precipitation of those minerals. In either case, brucite may precipitate at low c/h within or near the spring vents, because of Mg addition from cold seawater.

The submarine carbonate minerals appear to form by processes similar to those that form vein carbonates and carbonate-cemented conglomerates within or downstream from ultramafic bodies (Barnes and O'Neil, 1969, 1971; Barnes et al., 1978). Such carbonates include aragonite, calcite, magnesian calcite, dolomite, proto-dolomite, hydromagnesite, and magnesite (Barnes and O'Neil, 1969; Neal and Stanger, 1984). These deposits form by mixing of the calcium hydroxide fluids with magnesium bicarbonate surface and shallow groundwater common in alpine ultramafic bodies (Barnes and O'Neil, 1969; Neal and Stanger, 1984), possibly in combination with uptake of atmospheric CO_2 (Clark and Fontes, 1990; Clark et al., 1992; Neal and Stanger, 1984). The temperatures of vein deposit formation are uncertain (Barnes and O'Neil, 1969; Neal and Stanger, 1984), but the presence of magnesite may indicate elevated temperature (Barnes and O'Neil, 1969). In any case, the common process in the genesis of these deposits is the introduction of bicarbonate, derived from seawater, groundwater, or the atmosphere, into Ca^{2+}-OH^- fluid products of serpentinization.

6. THE RODINGITE ASSEMBLAGE AT 300°C

Two simulations assess the reaction of gabbroic/basaltic rocks with the Ca- and Al-rich serpentinization fluid obtained at log w/r = 0.4 at 300°C and P = 100 bar (Table 2). First, a pyroxene-bearing gabbro (Table 3) is added to the fluid at

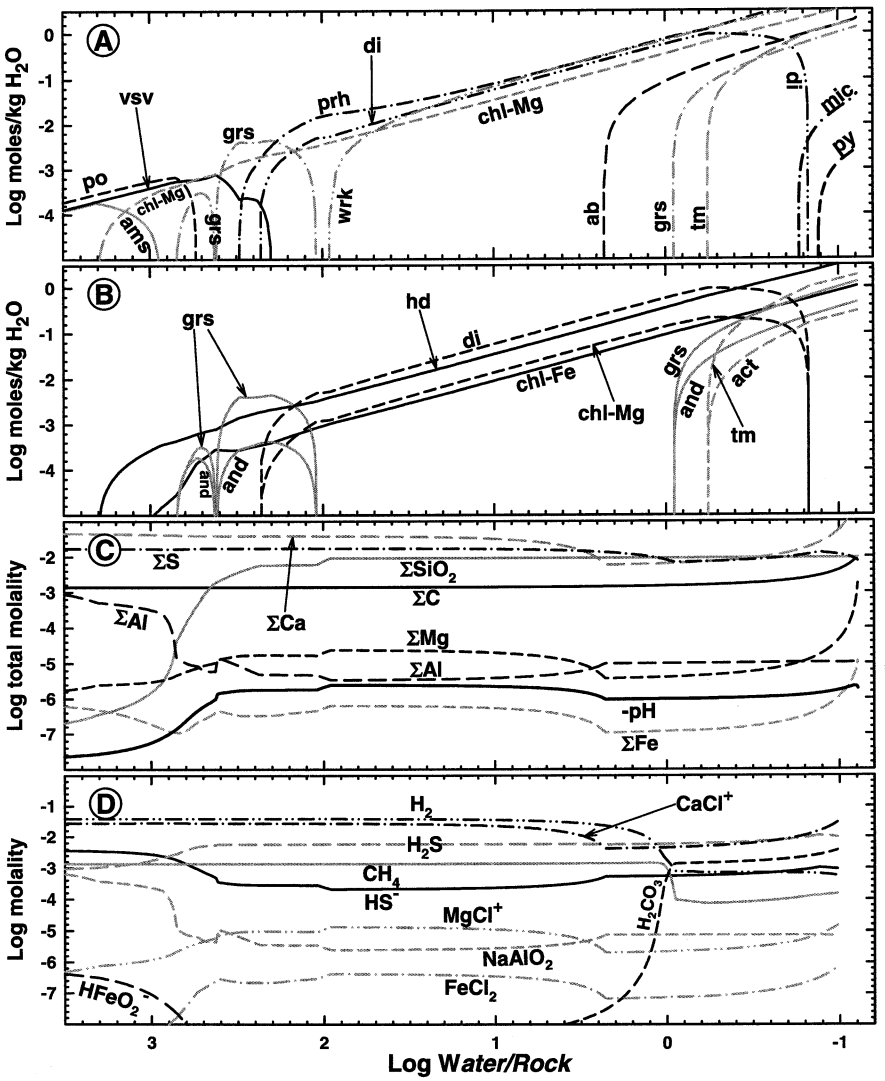

Fig. 6. Reaction zone metasomatism at 300°C of pyroxene-rich gabbro (Table 3), by the fluid product of serpentinization at log w/r = 0.4 (Table 2). A key to the mineral abbreviations is given in Table 1. a) Minerals. b) Solid solution compositions. c) Total concentration of aqueous components. d) Concentration of selected species.

300°C. Vesuvianite, pyrrhotite, and amesite precipitate with the first increment of added rock (off scale left, Fig. 6A). Amesite is replaced by chlorite that persists to dry-up. With decreasing w/r, the three dominant minerals evolve from vsv–chl–grs, through grs–chl–prh, prh–grs–di, prh–di–chl, and prh–di–wrk. Prehnite, diopside and wairakite quantities are subequal over a wide range of w/r. At the smallest w/r diopside dissolves out, and the assemblage is dominated by prehnite, wairakite, chlorite, with lesser albite, grossular, microcline and pyrite. Garnet, pyroxene, amphibole, and chlorite solid solutions are dominated by the endmembers grossular, diopside, tremolite, and Mg-chlorite, respectively (Fig. 6B). The minerals are characteristic of rodingites except wairakite, which may occur because of the absence of thermodynamic data for more-stable hydrogrossular. However, wairakite occurs in mafic rocks that have undergone zeolite facies metamorphism, and most of the other minerals are characteristic of either prehnite-pumpellyite or albite-epidote hornfels facies (Yardley, 1989); the assemblage, pressure, and temperature are consistent with transition between the three facies. Further, the fluid becomes much less alkaline and is depleted in Ca at small w/r (Figs. 6C,D), losing its potential to form rodingite, and typical metamorphic minerals might be expected.

With decreasing w/r, the fluid evolves to lower pH and higher concentrations of SiO_2 and Al (Figs. 6C,D). Ca decreases until albite-in, then increases until alteration dry-up; however, total Ca mass in the remaining fluid is less than in the initial fluid, indicating a net transfer of Ca into the alteration assemblage. Most of the decrease in Al occurs around log w/r 3.0, crudely mirroring the pH curve, and results from precipitation of vesuvianite, clinochlore, and grossular. The concentration of SiO_2 increases by almost five orders of magnitude, becoming near-constant at wairakite-in near log w/r = 2.0. The alteration reactions neutralize alkalinity, and the pH is ~5.6 at

Table 5. Initial pH, final pH, and pH resulting from mineral buffers in serpentinization models.

	initial	caminite	serpentine	brucite	calcic phase	final
[1]simplified model, 25°C	5.7		9.4	10.3	11.6	14.0
[1]meteoric, 25°C	5.7		9.4	10.3	11.6	14.0
[1]seawater, 25°C	7.0		8.0	9.2	10.8	11.2
[1]meteoric, 100°C	5.7		7.9	8.4	9.6	12.1
[1]seawater, 100°C	6.2		6.5	7.4	8.9	9.2
[2]seawater, 300°C	5.2	5.2		5.4	7.8	8.2

1. Serpentine phase is chrysotile, calcic phase is andradite-grossular solid solution.
2. Serpentine phase is antigorite, calcic phase is portlandite.

dry-up, almost two units less than in the initial fluid, and producing an assemblage characteristic of the metamorphic facies described above.

A second simulation (not shown in figures) uses an Al-rich norite (Table 3), to examine the alteration effects upon a protolith with greater alumina content; at log w/r less than ~1, the three dominant minerals are clinozoisite, albite, and wairakite, in contrast to prehnite, wairakite, and diopside described above. At higher w/r, the assemblage contains diaspore instead of amesite, and clinozoisite, in addition to grs, vsv, chl, and po that are common to both models. The changes in fluid composition resemble closely those for the model of rodingitization of the pyroxene gabbro.

The computed mineral assemblages show some significant differences from those in natural rodingites. Natural rodingites are generally dominated by Ca-rich garnet (hydrogrossular, grossular, andradite), with lesser diopside, epidote, tremolite, vesuvianite, prehnite, chlorite (Coleman, 1967; Rice, 1983; Schandl et al., 1989; Wares and Martin, 1980), xonotlite (Frost, 1975; Rice, 1983), clintonite (Rice, 1983), titanite, phlogopite (Schandl et al., 1989), and microcline (Wares and Martin, 1980). In a submarine setting (Ocean Drilling Program, site 895), incipient rodingitization yields prehnite, tremolite, chlorite, hydrogrossular, thomsonite, kaolinite, boehmite, diopside, chlorite, mixed layer chlorite/smectite, and iron hydroxides (Früh-Green et al., 1996). In general, epidote-clinozoisite forms at the earliest stages of alteration, and is replaced by hydrogrossular and prehnite (Schandl et al., 1989). In contrast, the computed assemblages are dominated by prehnite, wairakite, and diopside in the first system, and by clinozoisite and wairakite in the more aluminous system. Likely reasons for the differences are the lack thermodynamic data for hydrogrossular, and that natural fluid products of serpentinization are likely less aluminous than the fluid used here, both limiting the degree to which the models approach observed assemblages. Also, the simulations are simplified in that they use a fixed amount of fluid, into which increasing amounts of rock are added. In contrast, natural rodingites may form by a process in which many pore volumes of fluid diffuse through a fixed volume of rock. Nevertheless, the models show the evolution of mineral assemblages depleted in SiO_2 and enriched in calcium, as for natural rodingites.

7. SUMMARY AND CONCLUSIONS

All of the serpentinization simulations with either meteoric water or seawater at sufficiently small w/r, yield an alteration assemblage dominated by serpentine, brucite, and magnetite, similar to serpentinites commonly observed in submarine environments (Aumento and Loubat, 1971; Früh-Green et al., 1996; Hébert et al., 1990; Mével and Stamoudi, 1996; Rona et al., 1987; Schandl and Gorton, 1995), and in terrestrial systems (Coleman, 1977; O'Hanley, 1996; O'Hanley and Dyar, 1993). The aqueous phase evolves with decreasing w/r to increased concentrations of calcium and hydroxide, and becomes hyperalkaline and highly reducing. The fundamental reason that reaction of water with ultramafic rock produces hyperalkaline fluid is that OH^- produced by dissolution of olivine and pyroxene is not counterbalanced by OH^- consumption by precipitation of serpentine minerals until the OH^- concentration becomes quite large—hyperalkaline; i.e., in the ultramafic composition system, there are no insoluble alteration minerals that form in the neutral pH range. In contrast, rocks that contain sufficient aluminum will form chlorite or aluminous lizardite, for example, which consumes the OH^- produced by olivine dissolution and holds pH in the neutral range. System reduction with consequent H_2 production results from oxidation of ferrous iron in olivine and pyroxene to ferric iron in magnetite. The chemical changes occur in seawater at lower w/r than in fresh water, because large initial amounts of bicarbonate and sulfate in seawater buffer against increase in pH and decrease in redox potential, respectively. The computed altered seawater at 300°C contains Ag, Au, Cu, Co, Ni, Pt, and Pd in small amounts, but sufficient to precipitate ore minerals bearing those elements when the fluid is cooled or if aqueous sulfide is removed or oxidized.

Simulations of submarine mixing of cold seawater with hyperalkaline hydrothermal vent fluid produced by serpentinization yield carbonate-dominated mineral assemblages. Brucite is a significant product at ratios of seawater to vent fluid up to 5.0, and brucite precipitation may be preferred at higher temperatures near the vents. With progressive mixing, the computed mineral assemblage evolves from brucite-dominated to calcite-dominated, similar to that reported for submarine, ultramafic rock-hosted, carbonate deposits precipitating at hydrothermal vents near the mid-Atlantic ridge (Kelley et al., 2001).

The mineral assemblages generated in the rodingite simulations are similar to observations of rodingites in both terrestrial (Coleman, 1967; Frost, 1975; Rice, 1983; Schandl et al., 1989) and marine environments (Früh-Green et al., 1996). Gabbroic or basaltic precursors are altered to assemblages enriched in calcium and depleted in silica, and dominated by Ca-Al-(OH)-silicates. The computed alteration assemblages, depending on w/r, are dominated by grossular or prehnite in alteration of pyroxene gabbro, and epidote-clinozoisite, prehnite or waira-

kite in alteration of highly aluminous norite. A significant difference from natural assemblages is that hydrogrossular is absent, because it is absent from the mineral thermodynamic data. These simulations support the hypothesis that rodingite mineral assemblages form as result of calcium metasomatism, and that calcium moves from ultramafic rock into country rock, carried by serpentinizing fluids.

Acknowledgments—This work is a refinement of part III of the first author's graduate thesis, and we offer our thanks to M. Alan Kays and Jack M. Rice for helpful discussions during the course of the earlier study. We also thank Fred Wicks, Yousif Kharaka, two anonymous reviewers, and GCA associate editor Ron Frost for helpful and detailed comments which led to substantial improvement of this manuscript.

Associate editor: B. R. Frost

REFERENCES

Abrajano T. A. and Pasteris J. D. (1989) Zambales ophiolite, Phillippines: II. Sulfide petrology of the critical zone of the Acoje Massif. *Contrib. Mineral Petrol.* **103,** 64–77.

Abrajano T. A., Sturchio N. C., Bohlke J. K., Poreda R. J., and Stevens C. M. (1988) Methane-hydrogen gas seeps, Zambales ophiolite, Philippines: Deep or shallow origin? *Chem. Geol.* **71,** 211–222.

Abrajano T. A., Sturchio N. C., Kennedy B. M., Lyon G. L., Muehlenbachs K., and Bohlke J. K. (1990) Geochemistry of reduced gas related to serpentinization of the Zambales Ophiolite, Philippines. *Appl. Geochem.* **5,** 625–630.

Alt J. C. and Shanks W. C., III. (1998) Sulfur in serpentinized oceanic peridotites: Serpentinization processes and microbial sulfate reduction. *J. Geophys. Res.* **103 (***B5***),** 9917–9929.

Arnórsson S. (1983) Chemical equilibria in Icelandic geothermal systems- implications for chemical geothermometry investigations. *Geothermics* **12,** 119–128.

Arnórsson S., Gunnlaugsson E., and Hördur S. (1983) The chemistry of geothermal waters in Iceland. II. Mineral equilibria and independent variables controlling water compositions. *Geochim. Cosmochim. Acta* **47,** 547–566.

Aumento F. and Loubat H. (1971) The Mid-Atlantic ridge near 45°N. XVI. Serpentinized ultramafic intrusions. *Can. J. Earth Sci.* **8,** 631–663.

Barnes I. and O'Neil J. R. (1971) Calcium-magnesium carbonate solid solutions from Holocene conglomerate cements and travertines in the Coast Range of California. *Geochim. Cosmochim. Acta* **35,** 699–718.

Barnes I. and O'Neil J. R. (1969) The relationship between fluids in some fresh alpine-type ultramafics and possible modern serpentinization, western United States. *Geol. Soc. Am. Bull.* **80,** 1947–1960.

Barnes I., O'Neil J. R., and Trescases J. J. (1978) Present day serpentinization in New Caledonia, Oman and Yugoslavia. *Geochim. Cosmochim. Acta* **42,** 144–145.

Bazin B., Brosse E., and Sommer F. (1997a) Reconstitution de la chimie des eaux de gisement en réservoir gréseux en vue d'une modélisation numérique de la diagenèse minrérale. *Bulletin de la Société géologique de France.* **168,** 231–242.

Bazin B., Brosse E., and Sommer F. (1997b) Chemistry of oil-field brines in relation to diagenesis of reservoirs 1. Use of mineral stability fields to reconstruct in situ water composition. Example of the Mahakam basin. *Marine and Petroleum Geology* **14,** 481–495.

Berndt M. E., Allen D. E., and Seyfried W. E. (1996) Reduction of CO_2 during serpentinization of olivine at 300°C and 500 bar. *Geology* **24,** 351–354.

Berner E. K. and Berner R. A. (1996) Global Environment: Water, Air, and Geochemical Cycles. Prentice Hall, Upper Saddle River, N.J.

Bernoulli D. and Weissert H. (1985) Sedimentary fabrics in Alpine ophicalcites, South Pennine Arosa Zone, Switzerland. *Geology* **13,** 755–758.

Bonatti E., Emiliani C., Ferrara G., Honnorez J., and Rydell H. (1974) Ultramafic-carbonate breccias from the equatorial Mid Atlantic Ridge. *Marine Geol.* **16,** 83–102.

Botto R. I. and Morrison G. H. (1976) Josephinite: A unique nickel-iron. *Am. J. Sci.* **276,** 241–274.

Bougault H., Charlou J.-L., Fouquet Y., Needham H. D., Vaslet N., Appriou P., Baptiste P. J., Rona P. A., Dmitriyev L., and Silantiyev S. (1993) Fast and slow spreading ridges: Structure and hydrothermal activity, ultramafic topographic highs, and CH_4 output. *J. Geophys. Res.* **98 (***B6***),** 9643–9651.

Charlou J.-L. and Donval J.-P. (1993) Hydrothermal methane venting between 12°N and, 26°N along the Mid-Atlantic Ridge. *J. Geophys. Res.* **98 (***B6***),** 9625–9642.

Charlou J. L., Bougault H., Appriou P., Nelsen T., and Rona P. (1991) Different TDM/CH_4 hydrothermal plume signatures: TAG site at 26°N and serpentinized ultrabasic diapir at 15°N on the Mid-Atlantic Ridge. *Geochim. Cosmochim. Acta* **55,** 3209–3222.

Charlou J. L., Fouquet Y., Bougault H., Donval J. P., Etoubleau J., Jean-Baptiste P., Dapoigny A., Appriou P., and Rona P. A. (1998) Intense CH_4 plumes generated by serpentinization of ultramafic rocks at the intersection of the 15°20′N fracture zone and the Mid-Atlantic Ridge. *Geochim. Cosmochim. Acta* **62,** 2323–2333.

Chernosky J. V., Jr., Berman R. G., and Bryndzia L. T. (1988) Stability, phase relations, and thermodynamic properties of chlorite and serpentine group minerals. In *Hydrous Phyllosilicates (Exclusive of Micas)* (ed. S. W. Bailey), pp. 295–346. Mineralogical Society of America, Chelsea, Mich.

Clark I. D. and Fontes J. C. (1990) Paleoclimatic reconstruction in northern Oman based on carbonates from hyperalkaline groundwaters. *Quaternary Res.* **33,** 320–336.

Clark I. D., Fontes J. C., and Peter F. (1992) Stable isotope disequilibria in travertine from high pH waters: Laboratory investigations and field observations from Oman. *Geochim. Cosmochim. Acta* **56,** 2041–2050.

Coleman R. G (1967) Low-temperature reaction zones and alpine ultramafic rocks of California, Oregon and Washington. *USGS Bull. 1247*, pp. 1–49.

Coleman R. G. (1977) Ophiolites: Ancient Oceanic Lithosphere? Springer-Verlag, New York.

Coulton A. J., Harper G. D., and O'Hanley D. S. (1995) Oceanic versus emplacement age serpentinization in the Josephine ophiolite: Implications for the nature of the Moho at intermediate and slow spreading ridges. *J. Geophys. Res.* **100 (***B11***),** 22245–22260.

Coveney R. M., Goebel E. B., Jr., Zeller E. J., Dreschhoff G. A. M., and Angino E. E. (1987) Serpentinization and the origin of hydrogen gas in Kansas. *AAPG Bull.* **71,** 39–48.

Deer W. A., Howie R. A., and Zussman J. (1992) An Introduction to the Rock-Forming Minerals. Longman, Essex.

Eckstrand O. R. (1975) The Dumont serpentinite: A model for control of nickeliferous opaque mineral assemblages by alteration reactions in ultramafic rock. *Econ. Geol.* **70,** 183–201.

Evans B. W. (1977) Metamorphism of Alpine Peridotite and Serpentinite. *Ann. Rev. Earth Planet Sci.* **5,** 397–447.

Filippidis A. (1985) Formation of Awaruite in the system Ni-Fe-Mg-Si-O-H-S and olivine hydration with NaOH solution, an experimental study. *Econ. Geol.* **80,** 1974–1980.

Frost B. R. (1975) Contact metamorphism of serpentinite, chloritic blackwall and rodingite at Paddy-Go-Easy Pass, central Cascades, Washington. *J. Petrol.* **16,** 272–313.

Frost R. B. (1985) On the stability of sulfides, oxides and native metals in serpentinite. *J. Petrol.* **26,** 31–63.

Früh-Green G. L., Plas A., and Lécuyer C. M. (1996) Petrologic and stable isotope constraints on hydrothermal alteration and serpentinization of the EPR shallow mantle at Hess Deep (Site 895). *Proceedings, ODP, Scientific Results.* **147,** 255–291.

Giggenbach W. F. (1980) Geothermal gas equilibria. *Geochim. Cosmochim. Acta* **44,** 2021–2032.

Giggenbach W. F. (1981) Geothermal mineral equilibria. *Geochim. Cosmochim. Acta* **45,** 393–410.

Giggenbach W. F. (1987) Redox processes governing the chemistry of fumarolic gas discharges from White Island, New Zealand. *Appl. Geochem.* **2,** 143–161.

Giggenbach W. F. (1993) Redox control of gas compositions in Philippine volcanic-hydrothermal systems. *Geothermics* **22,** 575–587.

Hébert R., Adamson A. C., and Komor S. C. (1990) Metamorphic petrology of ODP Leg 109, Hole 670A serpentinized peridotites:

Serpentinization processes at a slow spreading ridge environment. *Proceedings, ODP, Scientific Results.* **106/109,** 103–115.

Helgeson H. C., Delany J. M., Nesbitt H. W., and Bird D. K. (1978) Summary and critique of the thermodynamic properties of rock-forming minerals. *Am. J. Sci.* **278-A,** 1–292.

Helgeson H. C., Kirkham D. H., and Flowers G. C. (1981) Theoretical prediction of the thermodynamic behavior of aqueous electrolytes at high pressures and temperatures: IV. Calculation of activity coefficients, osmotic coefficients, and apparent molal and standard and relative partial molal properties to 600°C and 5kb. *Am. J. Sci.* **281,** 1249–1516.

Hem J. D (1985) Study and interpretation of the chemical characteristics of natural water. *USGS Water-Supply Paper 2254.* 264 pp.

Holland T. J. B. and Powell R. (1998) An internally consistent thermodynamic data set for phases of petrological interest. *J. Metamorph. Geol.* **16,** 309–343.

Holm N. G. and Charlou J.-L. (2001) Initial indications of abiotic formation of hydrocarbons in the Rainbow ultramafic hydrothermal system, Mid-Atlantic Ridge. *Earth Planet Sci. Lett.* **191,** 1–8.

Kelley D. S. and Früh-Green G. L. (1999) Abiogenic methane in deep-seated mid-ocean ridge environments: Insights from stable isotope analyses. *J. Geophys. Res.* **104 (***B5***),** 10439–10460.

Kelley D. S., Karson J. A., Blackman D. K., Früh-Green G. L., Butterfield D. A., Lilley M. D., Olson E. J., Schrenk M. O., Roe K. K., Lebon G. T., Rivizzigno P. A., and Party A.-S. (2001) An off-axis hydrothermal vent field near the Mid-Atlantic Ridge at 30°N. *Nature* **412,** 145–149.

Knipper A. L. (1978) Ophicalcites and certain other types of breccias accompanying the pre-orogenic development of the ophiolite complex. *Geotectonics* **12,** 112–121.

Lorand J. P. (1987) Cu-Fe-Ni-S mineral assemblages in upper-mantle peridotites from the Table Mountain and Blow-Me-Down Mountain ophiolite massifs (Bay of Islands Area, Newfoundland): Their relationships with fluids and silicate melts. *Lithos* **20,** 59–76.

Macdonald A. H. and Fyfe W. S. (1985) Rate of serpentinization in seafloor environments. *Tectonophysics* **116,** 123–135.

McCollom T. M. and Seewald J. S. (2001) A reassessment of the potential for reduction of dissolved CO_2 to hydrocarbons during the serpentinization of olivine. *Geochim. Cosmochim. Acta* **65,** 3769–3778.

Mével C. and Stamoudi C. (1996) Hydrothermal alteration of the upper-mantle section at Hess Deep. *Proceedings, ODP, Scientific Results.* **147,** 293–309.

Neal C. and Stanger G. (1983) Hydrogen generation from mantle source rocks in Oman. *Earth Planet. Sci. Lett.* **66,** 315–320.

Neal C. and Stanger G. (1984) Calcium and magnesium hydroxide precipitation from alkaline groundwaters in Oman, and their significance to the process of serpentinization. *Mineral. Mag.* **48,** 237–241.

O'Hanley D. S. (1996) Serpentinites. Oxford University Press, New York.

O'Hanley D. S. and Dyar M. D. (1993) The composition of lizardite 1T and the formation of magnetite in serpentinites. *Am. Min.* **78,** 391–404.

O'Hanley D. S., Chernosky J. V., and Wicks F. J. (1989) The stability of lizardite and chrysotile. *Can. Min.* **27,** 483–493.

Ohmoto H. and Lasaga A. C. (1982) Kinetics of reactions between aqueous sulfates and sulfides in hydrothermal systems. *Geochim. Cosmochim. Acta* **46,** 1727–1745.

Palandri J. L. and Reed M. H. (2001) Reconstruction of in situ composition of sedimentary formation waters. *Geochim. Cosmochim. Acta* **65,** 1741–1767.

Pang Z. and Reed M. H. (1998) Theoretical chemical thermometry on geothermal waters: Problems and methods. *Geochim. Cosmochim. Acta* **62,** 1082–1091.

Prichard H. M. (1979) A petrographic study of the process of serpentinisation in ophiolites and the ocean crust. *Contrib. Mineral Petrol.* **68,** 231–241.

Reed M. H. (1982) Calculation of multicomponent chemical equilibria and reaction processes in systems involving minerals, gases and an aqueous phase. *Geochim. Cosmochim. Acta* **46,** 513–528.

Reed M. H. (1983) Seawater-basalt reaction and the origin of greenstones and related ore deposits. *Econ. Geol.* **78,** 466–485.

Reed M. H. (1997) Hydrothermal alteration and its relationship to ore field composition. In *Geochemistry of Hydrothermal Ore Deposits* (ed. H. L. Barnes), pp. 303–366. John Wiley & Sons, New York.

Reed M. H. (1998) Calculation of simultaneous chemical equilibria in aqueous-mineral-gas systems and its application to modeling hydrothermal processes. In *Techniques in Hydrothermal Ore Deposits Geology* (eds. J. Richards and P. Larson), pp. 109–124. Economic Geology.

Reed M. H. and Spycher N. F. (1984) Calculation of pH and mineral equilibria in hydrothermal waters with application to geothermometry and studies of boiling and dilution. *Geochim. Cosmochim. Acta* **48,** 1479–1492.

Rice J. M. (1983) Metamorphism of rodingites: Part I. Phase relations in a portion of the system CaO-MgO-Al_2O_3-CO_2-H_2O. *Am. J. Sci.* **283-A,** 121–150.

Rona P. A., Widenfalk L., and Bostroem K. (1987) Serpentinized ultramafics and hydrothermal activity at the Mid-Atlantic Ridge crest near 15°N. *J. Geophys. Res.* **92 (***B2***),** 1417–1427.

Rona P. A., Bougault H., Charlou J. L., Appriou P., Nelson T. A., Trefry J. H., Eberhart G. L., Barone A., and Needham H. D. (1992) Hydrothermal circulation, serpentinization, and degassing at a rift valley-fracture zone intersection: Mid-Atlantic Ridge near 15°N, 45°W. *Geology* **20,** 783–786.

Schandl E. S. and Gorton M. P. (1995) Phyllosilicate alteration of olivine in the lower sheeted dike complex, Leg 140, Hole 504B. *Proceedings, ODP, Scientific Results.* **137/140,** 207–216.

Schandl E. S., O'Hanley D. S., and Wicks F. J. (1989) Rodingites in serpentinized ultramafic rocks of the Abitibi Greenstone Belt, Ontario. *Can. Min.* **27,** 579–591.

Schroeder T., John B., and Frost B. R. (2002) Geologic implications of seawater circulation through peridotite exposed at slow-spreading mid-ocean ridges. *Geology* **30,** 367–370.

Seyfried W. E., Jr. and Mottl M. J. (1982) Hydrothermal alteration of basalt by seawater under seawater-dominated conditions. *Geochim. Cosmochim. Acta* **46,** 985–1002.

Spycher N. F. and Reed M. H. (1988) Fugacity coefficients of H_2, CO_2, CH_4, H_2O and of H_2O-CO_2-CH_4 mixtures: A virial equation treatment for moderate pressures and temperatures applicable to calculations of hydrothermal boiling. *Geochim. Cosmochim. Acta* **52,** 739–749.

Stefánsson A. and Arnórsson S. (2002) Gas pressures and redox reactions in geothermal fluids in Iceland. *Chem. Geol.* **190,** 251–271.

Tanger J. C., IV and Helgeson H. C. (1988) Calculation of the thermodynamic and transport properties of aqueous species at high temperatures and pressures: Revised equations of state for the standard and partial molal quantities of ions and electrolytes. *Am. J. Sci.* **288,** 19–98.

Trommsdorff V. and Evans B. W. (1977) Antigorite-ophicarbonates: Contact metamorphism in Valmalenco, Italy. *Contrib. Mineral Petrol.* **62,** 301–312.

Ulmer P. and Trommsdorff V. (1995) Serpentine stability to mantle depths and subduction-related volcanism. *Science* **268,** 858–861.

Wares R. P. and Martin R. F. (1980) Rodingitization of granite and serpentinite in the Jeffrey Mine, Asbestos, Quebec. *Can. Min.* **18,** 231–240.

Wedepohl K. H. (1969–1978) *Handbook of Geochemistry*. Springer, Berlin.

Wetzel L. R. and Shock E. L. (2000) Distinguishing ultramafic- from basalt-hosted submarine hydrothermal systems by comparing calculated vent fluid compositions. *J. Geophys. Res.* **105 (***B4***),** 8319–8340.

Wicks F. J. and O'Hanley D. S. (1988) Serpentine minerals: Structure and petrology. In *Hydrous Phyllosilicates (Exclusive of Micas)* (ed. S. W. Bailey), pp. 91–167. Mineralogical Society of America, Chelsea, Mich.

Wolery T. J (1992) EQ3/6, A Software Package for Geochemical Modeling of Aqueous Systems. Lawrence Livermore National Laboratory.

Yardley B. W. D. (1989) An Introduction to Metamorphic Petrology. Longman Scientific and Technical/John Wiley & Sons, New York.